ANNUAL REVIEWS

Annual Review of Fluid Mechanics

Fundamental Fluid Dynamics Challenges in Inkjet Printing

Detlef Lohse[1,2]

[1]Physics of Fluids Group and Max Planck Center for Complex Fluid Dynamics, Department of Science and Technology, J.M. Burgers Center for Fluid Dynamics, and MESA+ Institute, University of Twente, Enschede, The Netherlands; email: d.lohse@utwente.nl

[2]Max Planck Institute for Dynamics and Self-Organization, Göttingen, Germany

Annu. Rev. Fluid Mech. 2022. 54:349–82

First published as a Review in Advance on October 20, 2021

The *Annual Review of Fluid Mechanics* is online at fluid.annualreviews.org

https://doi.org/10.1146/annurev-fluid-022321-114001

Keywords

inkjet printing, piezoacoustics, nozzle, jetting, drops, pinch-off, impact, drop coalescence, drop–film interaction, drop evaporation, Marangoni flow, physicochemical hydrodynamics

Abstract

Inkjet printing is the most widespread technological application of microfluidics. It is characterized by its high drop productivity, small volumes, and extreme reproducibility. This review gives a synopsis of the fluid dynamics of inkjet printing and discusses the main challenges for present and future research. These lie both on the printhead side—namely, the detailed flow inside the printhead, entrained bubbles, the meniscus dynamics, wetting phenomena at the nozzle plate, and jet formation—and on the receiving substrate side—namely, droplet impact, merging, wetting of the substrate, droplet evaporation, and drying. In most cases the droplets are multicomponent, displaying rich physicochemical hydrodynamic phenomena. The challenges on the printhead side and on the receiving substrate side are interwoven, as optimizing the process and the materials with respect to either side alone is not enough: As the same ink (or other jetted liquid) is used and as droplet frequency and size matter on both sides, the process must be optimized as a whole.

INTRODUCTION

Inkjet printing is the most widespread technological application of microfluidics. It is characterized by its high drop productivity, small volumes, and extreme reproducibility. Besides the graphic printing industry, this drop deposition technique is used in dozens of other applications, such as solar cell printing, printing of microlenses, fuel cells, batteries, light-emitting displays, flat-panel and liquid-crystal displays, circuit boards, rapid prototyping, additive manufacturing, and even printing of polymers, DNA, proteins, and living tissues (Le 1998, Sirringhaus et al. 2000, Williams 2006, Dijksman et al. 2007, Wijshoff 2010, Hoath 2016, Dijksman 2019). Some of these applications require 100% reliability: For example, if inkjet printing is applied to create electronics (Kateri et al. 2003), missing a single drop can already lead to circuit failures. Similar precision is required in medical diagnostics and precision dosage of drugs (Daly et al. 2015).

There are two main principles to generate droplets, namely continuous inkjet printing and drop-on-demand (DOD) techniques. Whereas in continuous inkjet printing, drops are continuously created thanks to the Rayleigh–Plateau instability of the jet and sorted afterward by deflecting them, only directing a fraction of them toward the substrate and recycling the rest, in DOD techniques the drops are generated on demand and jetted toward the substrate. To do so, an actuation pressure has to be built up in the ink channel, and this is achieved either by piezoacoustic actuators (piezoelectric DOD) or thermally by nucleating a small vapor bubble with a thin-film heater (thermal DOD). While this latter technique is mostly used for inkjet printers at home, for high-end printing technologies piezoelectric DOD is the preferred and more flexible technique: The drop volume and velocity can easily be modulated with the piezoacoustic pulse width and strength, high jetting rates can be achieved, and thanks to the MEMS (micro-electromechanical systems) technology, such printheads can today be manufactured cheaply. This review will therefore focus on the piezoacoustic DOD inkjet printing technique.

A time series of stroboscopically imaged jetted droplets generated with the DOD technique is shown in **Figure 1**, conveying a visual idea of the high degree of reproducibility which can and must be achieved. At the same time the figure also reveals the aesthetic beauty of the droplet jetting process. The stability of the process is the more remarkable given the fast timescale and the small length scale of the printing process, namely for piezoacoustic DOD inkjet printing normally in the range of 10–100 kHz and for a droplet volume of ~0.5–100 pL. A typical droplet diameter is 20 μm, corresponding to 4 pL, and a typical droplet velocity is 10 m/s.

The fluid dynamics challenges in inkjet printing lie both on the printhead side—namely, the piezoacoustic actuation and the detailed flow inside the printhead, entrained bubbles, the meniscus dynamics, wetting phenomena at the nozzle plate, and jet formation—and on the receiving substrate side—namely, droplet impact, merging, the wetting of the substrate, droplet evaporation, and drying. These challenges are interwoven, as optimizing the process and the materials with respect to either the printhead side or the receiving substrate side is not enough: As the same ink is used and as droplet frequency, velocity, and size matter on both sides, the process must be optimized as a whole. One example for conflicting requirements from the printhead side on the one hand and from the receiving substrate or, more specifically, the paper side on the other hand is the volatility of the ink: At the nozzle, it would be preferable if the evaporation of ink were avoided to prevent nozzle clogging, but on the paper side, fast evaporation of ink is desirable to enable productive printing and to prevent paper deformation.

Synopsis of the Jetting Process

The series of events in inkjet printing is visualized in **Figure 2**, in which we identify seven fundamental fluid dynamics challenges:

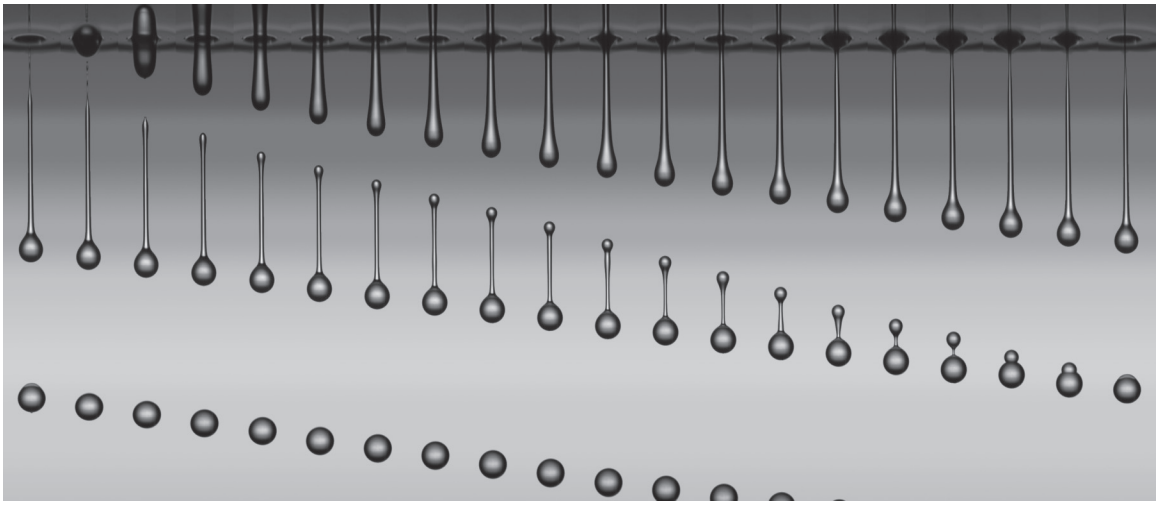

Figure 1

Time series of jetted ink droplets in piezoacoustic inkjet printing, stroboscopically recorded with single-flash photography. (*Left to right*) Multiple images of single droplets with a delay of 3 μs between the individual droplets. Here the opening radius of the nozzle is 15 μm and the diameter of the droplet 23 μm, which corresponds to a droplet volume of 11 pL. The final velocity of the droplet is 4 m/s. The figure illustrates the imaging quality and the absence of motion blur due to the use of the 8-ns iLIF (illumination by laser-induced fluorescence) technique. Figure reproduced with permission from van der Bos et al. (2014).

- The process starts in the ink chamber (❶) in the printhead, where pressure is periodically built up with a piezoacoustic actuator; in response, ink is pressed out of the nozzle, provided the pressure is large enough.
- Under certain conditions bubbles (❷) can be entrained into the nozzle of the printhead, seriously disturbing the printing process, as the pressure pulse is then absorbed by the bubble, rather than leading to jetting.
- The jetting frequency is in fact limited by fluid dynamical instabilities that can occur at the edge (❸) of the nozzle, where the flow inside the nozzle interacts with that on the nozzle

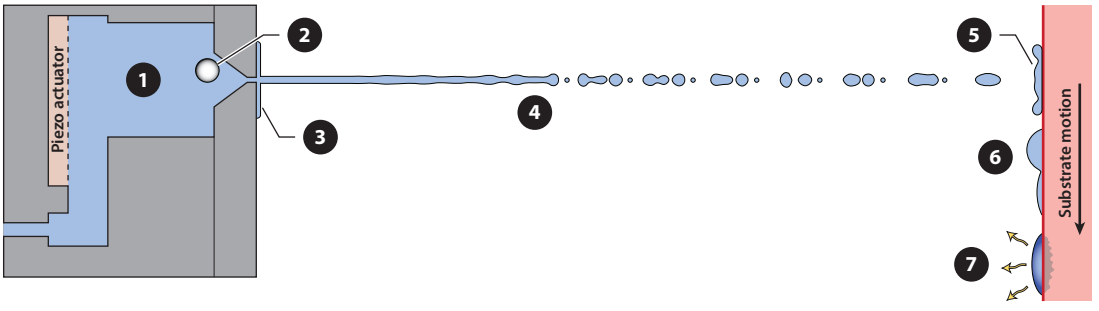

Figure 2

Visualization of the series of events and physical processes in inkjet printing, from the ink–piezo actuator interaction (*left*), via ink jetting (*middle*), to the interaction between ink and the receiving substrate (*right*). The circled numbers refer to the seven fundamental fluid dynamics challenges referenced in the sections of this review: (❶) the flow and acoustics in the inkjet printhead; (❷) bubbles that are entrained into the nozzle and disturb the printing operation; (❸) the wetting dynamics on the nozzle plate, including the meniscus, droplet, and film dynamics; (❹) the jetting process, including satellite formation; (❺) the drop impact and spreading on the substrate; (❻) drop coalescence, drop–film interaction, and ink–paper interaction; and (❼) the evaporation and solidification of the ink.

plate. The geometry of the nozzle and the wetting properties of the nozzle plate are crucial for achieving optimal stability, as they affect the fluid dynamics of the oscillating meniscus.

- For large enough pressures, droplets form at the tip of the jet, detach, and fly toward the substrate. When exactly they detach (❹) and what size they have depend not only on the driving pressure, driving frequency, and geometry but also on the material properties of the ink.
- Finally, the drop impacts on the substrate and spreads sideways (❺).
- Often the impact is not on a dry surface but on a thin film of ink or a coating layer that had been previously deposited, or on/close to droplets that had previously landed on the substrate. There, drop–film and drop–drop interactions such as merging become very crucial (❻). Often these interactions determine the quality of the print. The interaction of the droplet with the substrate can also be relevant as with, e.g., paper, in which ink intrudes and is absorbed.
- Finally, in the case of aqueous inks the droplet will partially evaporate (❼) and leave behind pigments, or in case of inks consisting of molten wax, it will solidify, thanks to cooling or to chemical reactions and cross-linking of some polymer. The optical appearance of the dried pattern is the final result and reflects the quality of the print. In any case, the drying process can take very long, up to hours or even days.

Here the circled numbers not only correspond to those in **Figure 2**, but also to those of the later sections of this review.

Control Parameters

The control and design parameters of inkjet printing are geometrical parameters such as the ink chamber volume and nozzle diameter and shape; the pressure amplitude and frequency and, more generally, the shape of the pressure pulse; the material properties of the ink such as the surface tension, viscosity, thermal diffusivity, density, and volatility; and the geometrical and material properties of the substrate. Most inks are not pure liquids but have a very complex composition, containing multiple liquids with different material properties, pigments, other colloidal particles, latex, cross-linkers, surfactants, and polymers. The ink can be either of aqueous or of organic character, and depending on this, solidification is achieved by evaporation, cooling down below the melting temperature, cross-linking triggered by ultraviolet (UV) radiation, or other chemical reactions. For inks with complex compositions further control parameters come into play, such as the relative mass or volume fractions of the different ingredients, and, in the case of colloidal particles, their size, shape, and chemical nature. This further complicates the printing process, leading to new, exciting, and rich physicochemical hydrodynamics phenomena in and between the droplets. For example, surfactants accumulate on the interface during the droplet-spreading process, leading to a time- and position-dependent surface tension, and pigments potentially cluster, leading to clogging in the nozzle. After the deposition of multicomponent droplets, certain ingredients of the liquid evaporate preferentially, leading to concentration gradients at the interface and thus gradients in the surface tension, resulting in Marangoni flows. These can also occur between droplets of two different liquids or with a droplet on a film of a different liquid.

As in all fields of fluid dynamics, it is very convenient and therefore common to express the control parameters for inkjet printing in terms of dimensionless numbers, which are ratios of different forces or time- or length scales. For better readability, we have summarized the most important dimensionless numbers in inkjet printing in the sidebar titled Dimensionless Numbers for Droplets in Inkjet Printing.

DIMENSIONLESS NUMBERS FOR DROPLETS IN INKJET PRINTING

Just as in other parts of fluid dynamics, in inkjet printing it is convenient and therefore common to express the ratio of the various forces (or time- or length scales) in terms of dimensionless numbers. The most relevant ones in inkjet printing are the **Reynolds number**, $Re = UR/\nu$, the ratio of inertial to viscous forces, where R is the droplet radius, U is the droplet velocity resulting from the pressure buildup in the ink channel, and ν is the kinematic viscosity of the ink; the **Weber number**, $We = \rho U^2 R/\sigma$, the ratio of inertial to capillary forces, where σ is the surface tension and ρ is the density of the liquid; the **capillary number**, $Ca = \eta U/\sigma = We/Re$, the ratio of viscous to capillary forces, where here $\eta = \nu\rho$ is the dynamic viscosity of the ink; and the **Ohnesorge number**, $Oh = \eta/\sqrt{\rho\sigma R} = We^{1/2}/Re$, the ratio of the viscous timescale to the capillary timescale. Obviously, only two of these four dimensionless parameters are independent. In general, on the small length scales of the droplets, gravity is not relevant, and therefore the corresponding dimensionless numbers such as the Bond number, the Froude number, or the Morton number do not play a role.

However, what can play a role are non-Newtonian properties of the ink. For viscoelastic liquids, these are partially characterized by the **Deborah number**, $De = \tau_r/\tau_c$, where τ_r is the relaxation timescale of the non-Newtonian liquid and $\tau_c = (\rho R^3/\sigma)^{1/2}$ is the capillary timescale.

The frequency Ω of the acoustic pulses driving the jetting in dimensionless form is expressed as the **Womersley number**, $Wo = L\sqrt{\Omega/\nu}$, where L is a characteristic length scale of the nozzle. Additionally, the surrounding air (or more generally, the surrounding gas) with its dynamic viscosity η_g and its density ρ_g plays a role, as it exerts friction on the flying droplet and an air layer has to be pushed away upon impact of the drop on the substrate. Its effect is expressed in terms of the **Stokes number**, $St = \rho RU/\eta_g = \rho Re/\rho_g$.

Once the ink is multicomponent, the diffusion of one component in another and, thus, the diffusivity D become important, giving rise to the **Péclet number**, $Pe = UR/D$, and the **Schmidt number**, $Sc = \nu/D$. Once thermal effects also come into play, the thermal diffusivity κ matters, or in dimensionless form, the **Prandtl number**, $Pr = \nu/\kappa$, or the **Lewis number**, $Le = \kappa/D$. Typically $Pr \sim 4$ and $Le \sim 400$, reflecting that the thermal diffusivity is much faster than the molecular one, and that for standard liquid inks thermal transport is slightly slower than viscous transport.

In the case of selective evaporation of one component or local cooling or heating of the droplets, Marangoni forces also come into play. The **Marangoni number**, $Ma = R\Delta\sigma/(\rho\nu D)$, compares the Marangoni forces with stabilizing viscous forces and stabilizing mass diffusion. The difference $\Delta\sigma$ in surface tension may be due to differences Δc in the composition of the liquid, where $c(\mathbf{x}, t)$ is the concentration field, or due to differences ΔT in the temperature of the liquid. Roughly, we have $\Delta\sigma \approx \partial_c\sigma\ \Delta c$, and similarly for the temperature, but note that in general the dependence $\sigma(c)$ is very nonlinear (Vazquez et al. 1995). In general, of course, σ is a function of T and c, and $\Delta\sigma \approx \partial_T\sigma|_c\Delta T + \partial_c\sigma|_T\Delta c$.

Finally, once also chemical reactions come into play, we also need the **Damköhler number** Da, which expresses the ratio between chemical reaction rate and (diffusive or convective) mass transport rate. We revisit these numbers below in the discussions of the various fluid dynamical effects of droplets in inkjet printing.

Objectives and Dilemmas in Inkjet Printing

In various inkjet applications, the objective is to reliably generate even smaller drops, to jet at ever higher frequencies, or to operate the device with more viscous materials. Smaller droplets and higher frequencies not only make piezoacoustic inkjet printers even more precise and faster but also open up various applications in biology, medicine, microfabrication, and chemistry. But what are the limits to achieving this?

The limiting conditions of the inkjet printing process are illustrated in **Figure 3**, which shows the domain for reliable inkjet printing in the parameter space of Reynolds number Re (representing

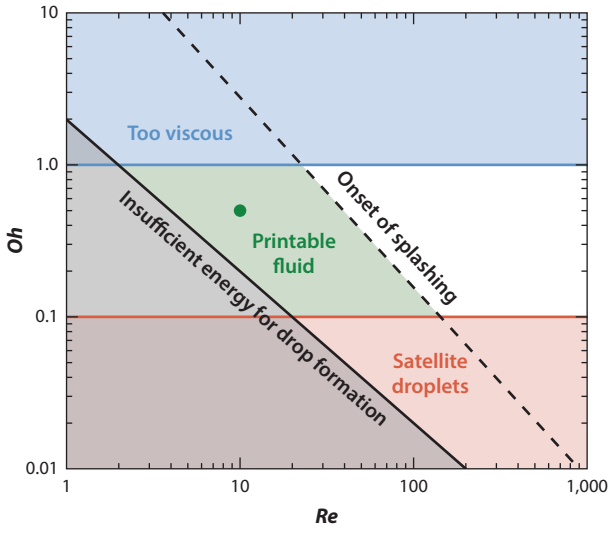

Figure 3

The operating regime for stable operation of drop-on-demand inkjet printing in the control parameter space of Ohnesorge number *Oh* versus Reynolds number *Re*. The criterion for a drop to possess sufficient kinetic energy to be ejected from the nozzle (end-pinching) is given by Lin & Reitz (1998) as Weber number $We_{\text{crit}} \geq 4$ or $Re \leq 2/Oh$. The criterion for the onset of splashing following impact is given by Derby (2010) as $OhRe^{5/4} \geq 50$. For too low surface tension, not only does end-pinching occur, but also the ink filament experiences a Rayleigh–Plateau or other type of instability and satellite droplets emerge. Here a horizontal red line signals the regime $Oh \leq 0.1$ for satellite droplet formation (Notz & Basaran 2004; Dong et al. 2006; Xu, Shi & An 2007). A typical example case that we repeatedly use in this review is a droplet diameter $2R = 20$ μm and a velocity $u = 10$ m/s. With $\rho = 1{,}000$ kg/m^3, $\nu = 10^{-5}$ m^2/s, and $\sigma = 0.05$ N/m as typical material properties for ink, this implies $Re = 10$ and $Oh = 0.5$ (shown as a green dot in the diagram), corresponding to $We = 25$ and capillary number $Ca = 0.25$. A similar diagram, but in the parameter space of $1/Oh$ versus We and including experimental data, is given by Liu & Derby (2019). Figure adapted with permission from McKinley & Renardy (2011).

the inkjet velocity and thus the pressure buildup in the ink chamber) and Ohnesorge number *Oh* (representing the material properties of the ink, i.e., the ratio between viscous and capillary timescales; see the sidebar titled Dimensionless Numbers for Droplets in Inkjet Printing). As can be seen, printing is only possible for intermediate Reynolds number and intermediate Ohnesorge number: For too small *Re*, the actuation is not strong enough to form droplets, i.e., to achieve a droplet pinch-off from the oscillating meniscus. In contrast, for too large *Re*, the droplet impacting on the substrate would splash, which is undesirable for precise printing. In the other direction of the parameter space, for too large *Oh* the ink is too viscous to be jetted through pressure buildup, but for too small *Oh*, the surface tension is strong enough to lead to satellite droplet formation through the Rayleigh–Plateau instability of the ink filament, which is also unwanted in controlled inkjet printing. The transitions between the various regimes follow scaling laws, which we explain in more detail below.

Another dilemma in inkjet printing is connected with the volatility of the ink or, in other words, with the time it takes the ink to dry. On the one hand, one would like the ink to dry quickly once it has landed on the substrate, so high volatility or fast solidification of the ink is desirable. On the other hand, if this holds, it also holds for ink on the nozzle plate and at the meniscus. This can lead to clogging of the nozzle or—in the case of selective evaporation of one component of the

ink—to concentration gradients at and around the nozzle, leading to differences in surface tension and thus to Marangoni flows. It can also lead to a modification in the ink viscosity and therefore to changes in the printability, with a strong bearing on reproducibility. Further dilemmas have been sketched by Clasen et al. (2012).

The fundamental fluid dynamical challenges in inkjet printing are to find a way out of all these dilemmas. This can be achieved by a compromise between the various requirements and by fine-tuning the control parameters. It can also consist of introducing new degrees of freedom into the problems: For example, for the first of the abovementioned dilemmas (strong enough actuation to overcome the capillary forces at the meniscus but weak enough actuation to avoid satellite droplets), a new degree of freedom is to add some polymers to the ink to introduce some elasticity, which delays the satellite formation. For the second of the abovementioned dilemmas (droplet solidification both on the substrate and around the nozzle), one way out is to employ inks consisting of molten wax and to operate the printhead at a temperature above the wax's melting temperature. Then, on the substrate side without heating, solidification sets in immediately.

Such work-arounds to the dilemmas and diverging requirements in inkjet printing often involve modifications of the ink itself. Indeed, modern commercial inks have an extremely complex, multicomponent composition, also containing pigments and surfactants. This complex multicomponent composition can again introduce various new challenges and effects, like the abovementioned selective evaporation of one or a few components, and the resulting Marangoni flows, inside the droplets. Optimizing the inkjet printing process therefore requires a good understanding of the physicochemical hydrodynamics of droplets far from equilibrium.

It is clear that the inkjet printing process is a multiscale problem. The timescales reach from the nanosecond timescale relevant at the pinch-off of the droplet to the timescales of the drying process, which can exceed weeks, or even to the timescales of the durability of the printed area, which in many applications must be years. Similarly, the length scales span from the nanometers of the droplet pinch-off process to tens of meters of the whole printing device or the printed areas.

Organization of the Review

We organize the review along the series of events sketched in **Figure 2** and described above, i.e., starting from the fluid dynamics in the printhead, via the nozzle dynamics and jetting process, to the impact, wetting, and drying process. The seven themes of **Figure 2** correspond to the next seven main sections of this review, which in the end is accompanied by an outlook and a list of open problems.

Another element of the review is the sidebars, which we use to introduce the reader to recurring definitions or methods: In the sidebar titled Dimensionless Numbers for Droplets in Inkjet Printing, we introduce the most relevant dimensionless numbers of the inkjet printing process, and the sidebars titled Modern Experimental Methods in Inkjet Printing and Numerical Methods in Inkjet Printing are used to explain new relevant experimental and numerical methods, respectively. The sidebar titled Quasi-Parallel Flow Approximations in Inkjet Printing briefly conveys the idea of quasi-parallel flow approximations and gives four examples where they are applied in the context of inkjet printing.

Inkjet printing is a multidisciplinary endeavor par excellence, covering not only fluid dynamics but also acoustics, chemistry, materials science, chemical and mechanical engineering, electronics, optics, signal processing, computer science, physics, and more. This review focuses on the fluid dynamics aspects, but touches upon many others, and emphasizes that the inkjet process—from the ink chamber to the drying process on the substrate—must be approached as a whole.

MODERN EXPERIMENTAL METHODS IN INKJET PRINTING

Up to about three decades ago, the traditional approach in industrial inkjet printing research was to exclusively focus on the final static result of the print, namely, by optical microscopy. With this, an optical resolution of the final print of about one micrometer could be achieved. With electron microscopy or X-ray microscopy one could go beyond this toward smaller scales.

However, it became increasingly clear that in order to make further progress in the understanding of the inkjet printing process, dynamical measurements would be necessary, and the advent of advanced **high-speed and ultrahigh-speed digital imaging** about two decades ago has made this possible (Thoroddsen et al. 2008). Nonetheless, it is still extremely challenging to visualize the jetting and breakup of inkjet-printed droplets, as they are very fast and very small: For any high-speed camera, for high frame rates a dichotomy between good temporal resolution and good spatial resolution becomes unavoidable (Versluis 2013). For a given frame rate, the minimal properly resolved length scale of a moving object is proportional to its velocity. The typical drop velocity for inkjet printing is 10 m/s, the meniscus speeds are above 20 m/s, and the typical diameter of a droplet is about 20 μm. To visualize the details of such dynamics, one requires a high-speed camera with frame rates up to 25 million frames per second. Ultrahigh-speed imaging is highly relevant not only for the jetting of the droplet but also for its impact and spreading on the substrate.

Alternatively, to overcome the challenges of ultrahigh-speed imaging, one can often take advantage of the generally very high reproducibility of the ink-jetting process and apply **stroboscopic techniques** (see, e.g., Hutchings et al. 2007). van der Bos et al. (2011b) developed the so-called iLIF (illumination by laser-induced fluorescence) technique, allowing for two sequential frames separated by 500 ns imaged with an illumination time of only 10 ns. This technique can reveal the details of the jetted droplets and of the meniscus motion up to the optical limit of the microscope (less than a micron) and has made the recording of the time series of jetted ink droplets in **Figure 1** possible (van der Bos et al. 2014).

If applied to the bottom view of impacting droplets on a transparent substrate, high-speed photography can also be connected with interferometric and total internal reflection imaging (Thoroddsen et al. 2003, Driscoll & Nagel 2011, Bouwhuis et al. 2012, Kolinski et al. 2012, van der Veen et al. 2012, Shirota et al. 2016) to allow for, respectively, micrometer and tens-of-nanometer resolution of the closing air pocket between the impacting droplet and the transparent substrate, or to spatially and temporarily resolve the early solidification of a liquid droplet on a supercooled substrate (Kant et al. 2020).

For the much slower evaporation process of the deposited drop or for droplets on the nozzle plate, less time resolution is required, but still very high spatial resolution is needed, and preferentially in 3D. Two relatively new techniques that have great potential for inkjet printing are **confocal microscopy** (Hell 2009), which allows for 3D visualizations of flow within droplets, and **digital holography microscopy (DHM)** (Garcia-Sucerquia et al. 2006), which can be seen as complementary to confocal microscopy, focusing on interfaces rather than on the bulk, as in standard confocal microscopy. In the context of inkjet printing, DHM is ideal for high-precision visualizations of thin (deforming) films and droplets with small contact angles.

There are many other very good reviews and even books on inkjet printing, with widely varying focuses aimed at readers from various disciplines with varying objectives. Here we would like to refer the reader to Wijshoff (2010) on the structure dynamics, acoustics, and fluid dynamics of the piezo inkjet printhead operation; Dijksman (2019) on the design of piezo inkjet printheads; de Gans et al. (2004) on the inkjet printing of polymers; Eggers (1997, 2005) on the fundamentals of the breakup of the jet and the resulting droplet formation; Basaran (2002) on the more applied aspects of these processes; Basaran et al. (2013) on the pinch-off and droplet formation in nonstandard inkjets with complex liquids as inks; Derby (2010) on the printing of functional and

NUMERICAL METHODS IN INKJET PRINTING

Any high-speed imaging of the inkjet printing process must be complemented by numerical and theoretical work, as only then can one achieve an understanding of the mechanism and make predictions for other control parameters. Commercial computational fluid dynamics codes such as Ansys/Fluent, Comsol, or Flow3D are helpful to gain an overview, but for several applications they have limitations, often presumably due to numerical grid resolution issues that sometimes lead to artifacts. Therefore, they should be cross-checked against and accompanied by scientific codes.

Many of the numerical approaches can be used both on the ink channel side to describe the meniscus dynamics, the entrained bubble, and the droplet jetting and pinch-off and, at the same time, on the receiving substrate side to describe the droplet impact and spreading. It is crucial that the scientific codes and methods be benchmarked against each other and against experimental observations.

Finite-element methods with sharp interface representations of the free surfaces are ideally suited for various applications in the context of inkjet printing, such as jetted droplets (Antonopoulou et al. 2020) or droplets with mass exchange, which occurs at evaporation (Diddens et al. 2017b). Both require a well-resolved interface with the surrounding phases, which can be achieved with a mesh that is always conforming with the interface and, thus, is adaptive. This requires comoving all mesh nodes accordingly with the interface, which can be done with a so-called arbitrary Lagrangian–Eulerian algorithm (Notz & Basaran 2004; Heil & Hazel 2006, 2011; Diddens 2017). Additionally, for multicomponent droplets or interfaces with surfactants, this technique has proven to be extremely versatile (Tan et al. 2016; Diddens et al. 2017b; Kamat et al. 2018, 2020; Li et al. 2019a,b), but the challenge remains to efficiently parallelize such codes.

A sharp interface can also be achieved with **level set methods**, which in the context of inkjet printing have been used, e.g., to study droplet jetting out of ink chambers (Zhong et al. 2018) or droplet oscillations (Wang et al. 2019).

The **volume of fluid (VOF) method** (Josserand et al. 2009, Popinet 2018) is an Eulerian scheme that tracks the interface (including surface tension) and in general allows for adaptive grid refinement. Implementations include Gerris and the updated version Basilisk, which is an open source multiphase flow solver. With respect to VOF methods implemented in commercial packages, Gerris has the major advantage of being open source, and thus it allows for precise control of the models used and the possibility of adding new specific features.

Phase-field (or diffuse-interface) models have emerged over the past years as a comprehensive and versatile modeling paradigm for multicomponent flows, enabling realistic descriptions of complicated physical phenomena such as evaporation and condensation (Gomez et al. 2010, Liu et al. 2013), topological changes of fluid–fluid interfaces due to coalescence and pinch-off (Jacqmin 1999, Kim et al. 2004), contact-line motion at fluid–solid interfaces (Seppecher 1996, Jacqmin 2000), and elastocapillary effects of complex fluids on elastic solid substrates (van Brummelen et al. 2016).

Lattice Boltzmann methods are based on coarse-grained versions of the molecular theory of fluids and allow for massive parallelization. They have been adapted to capillary phenomena, surface wetting, and suspension droplets, including phase transitions such as evaporating droplets (Aidun & Clausen 2010, Harting et al. 2014, Hessling et al. 2017).

structural materials and the formation of drops of complex fluids; Le (1998), Martin et al. (2008), and Castrejon-Pita et al. (2013) on the technological aspects of inkjet printing; Wijshoff (2018) on various types of drop dynamics during the inkjet printing process; Josserand & Thoroddsen (2016) on droplet impact on a solid surface; Yarin (2006) and Yarin et al. (2017) on drop impact phenomena on solids and thin films; Quéré (2008) and Bonn et al. (2009) on the wetting and spreading of liquids on substrates; Cazabat & Guéna (2010) and Erbil (2012) on the evaporation of single-component liquid droplets; Brutin & Starov (2018) and Zang et al. (2019) on single- and

QUASI-PARALLEL FLOW APPROXIMATIONS IN INKJET PRINTING

Quasi-parallel flow approximations of the Navier–Stokes equations with their respective boundary conditions are extremely powerful in various situations in inkjet printing. Mathematically speaking, they can be seen as **long wave expansions** (Eggers 1997, Oron et al. 1997). They can be applied when the flow velocity in one direction is much larger than in the other ones or, correspondingly, when the flow geometry is such that the spatial extension in one direction is much smaller than in the other ones. Here we briefly sketch four examples in the context of inkjet printing.

The jetting flow velocity is much faster than the flow velocity in the direction perpendicular to the jetting direction (see the section on challenge ❹ below). In this context the quasi-parallel flow approximation is called **slender jet approximation**, thanks to which the Navier–Stokes equations and the Laplace equation for the free interface can be simplified to two coupled partial differential equations for the radius of the jet and for the liquid velocity, as functions both of the axial distance and of time (Eggers 1997, Eggers & Villermaux 2008). Obviously, this breaks down if, for fixed axial position, the interface is no longer single valued, but is instead three valued, due to overhanging structures like bulky droplets close to a pinch-off position. For a detailed comparison between the full simulation and the slender jet approximation (see, e.g., Ambravaneswaran et al. 2002).

Just before drop impact, the ink spreads radially outward, skating on a very thin film of air that can be treated within a **thin film approximation** or **lubrication approximation** (Mandre et al. 2009, Bouwhuis et al. 2012, Mandre & Brenner 2012) (see the section on challenge ❺). Here, remarkably, one can apply the viscous lubrication approximation for the thin air film between the drop and the substrate, as its thinness implies a very small Reynolds number.

After touchdown of the droplet, again the thin film equations (Oron et al. 1997, Craster & Matar 2009) can be used to describe droplet spreading on the substrate or on a thin film (Gaver & Grotberg 1992, Bonn et al. 2009) and wetting phenomena (Snoeijer & Andreotti 2013), including droplet coalescence (see the sections on challenges ❺ and ❻). This also holds for wetting phenomena and drops with small contact angles on the nozzle plate (see the section on challenge ❸).

Finally, for small contact angles, i.e., for very small heights of the droplet as compared to its lateral extension, the droplet evaporation (see the section on challenge ❼) can also be described within a lubrication approximation (Deegan et al. 1997, Marin et al. 2011, Diddens et al. 2017a), as then the flow velocity parallel to the substrate is dominant.

multiple-component drop evaporation, including application aspects; Sefiane (2014) on patterns from drying droplets; and Lohse & Zhang (2020) on the physicochemical hydrodynamics of multicomponent droplets, including their evaporation. Finally, we mention the handbooks by Hoath (2016) and Zapka (2017).

CHALLENGE ❶: FLUID DYNAMICS AND ACOUSTICS IN THE DROP-ON-DEMAND INKJET PRINTHEAD

The most controllable inkjet printheads are based on piezoelectric devices. In such devices (Dijksman 1984, 1999; Antobe & Wallace 2002; Feng 2002; Shin et al. 2003; Magen & Gottlieb 2004; Meacham et al. 2005; Le 1998) a voltage pulse applied to a piezoelectric element causes it and thus the ink-filled channel to deform, thereby creating a pressure wave in the ink. Fluid acoustics (Tijdeman 1975) is involved to guide the waveform energy toward the nozzle (typically 20–30 μm in diameter) and to create pressure and velocity profiles needed for the droplet jetting process. The whole process from the electrical signal at the piezo actuator to its mechanical deformation, the resulting pressure buildup, and, finally, to the jetting is schematically shown in **Figure 4*a***, which also sketches a typical piezo inkjet channel. A commercial printhead consists of

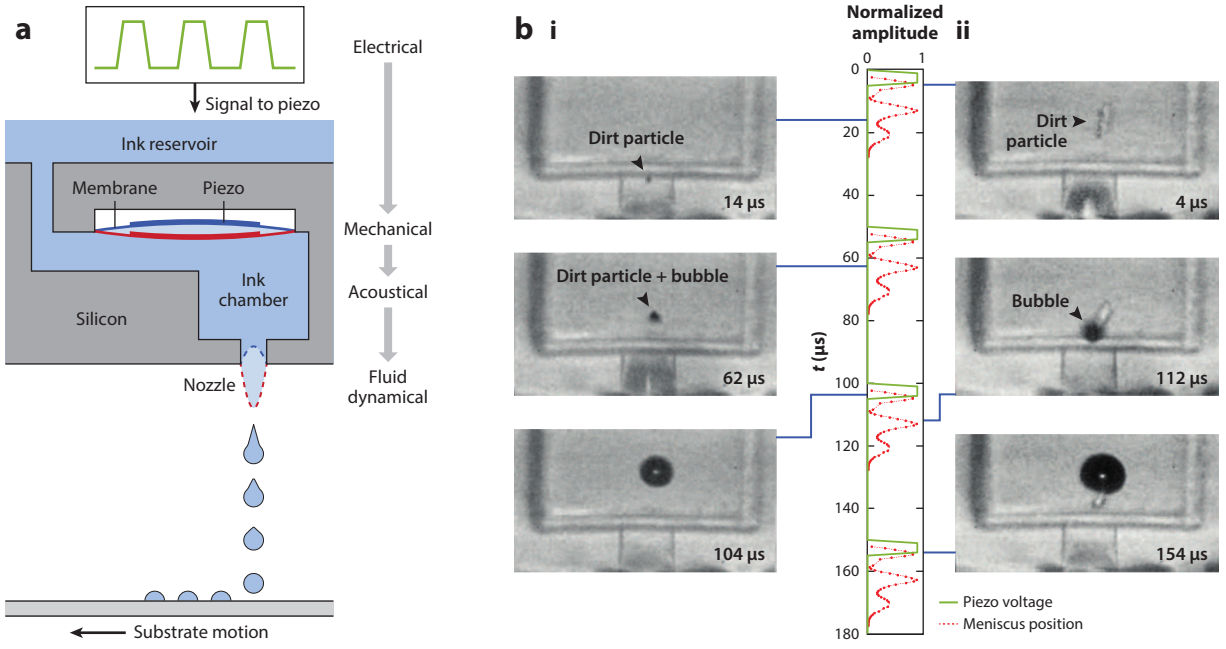

Figure 4

(*a*) Side view of a MEMS (micro-electromechanical systems) piezoacoustic inkjet channel, showing the principle of piezoacoustic inkjet printers: The electrical signal applied to the piezo actuator is transferred to a mechanical deformation, which leads to a pressure buildup in the ink chamber and, if large enough, finally to the ejection of a droplet, which is jetted toward a substrate. The membrane connected to the piezo is shown at pressure maximum in red and at pressure minimum in dark blue. The ink (*light blue*), coming from the reservoir, enters through a restriction, from where it flows into the actuation ink chamber. Below the actuation chamber a feedthrough is placed, after which the nozzle (with a diameter and length typically around 20–30 µm) is reached. (*b*) Bubble entrainment in the inkjet channel. Subpanels *i* and *ii* show typical bubble nucleation events, in subpanel *i* from a dirt particle entering the nozzle from outside, and in subpanel *ii* from a dirt particle floating inside the ink channel. The corresponding timing of the piezo actuation pulse and the meniscus position can be seen from the pressure signal and the meniscus position shown between subpanels *i* and *ii*. Figure adapted with permission from Fraters et al. (2019b).

thousands of such channels. The piezo actuators are made with a thin layer deposition technique (Brünahl & Grishin 2002, Funakubo et al. 2012). The advantages of the piezoacoustic MEMS devices are the very high printing precision (i.e., small drops), the very fast printing rate, and the low production costs. Note that the dependence between the amplitude and frequency of the electrical signal at the piezo actuator and the resulting pressure amplitude, and, thus, the droplet volume and velocity, is highly nonlinear, and resonances play a major role (Wijshoff 2010).

What are the typical acoustic pressure amplitudes which are required for jetting the droplets? Following Wijshoff (2010), we take as example a nozzle diameter of $2R_n = 30$ µm, corresponding cross section A_n, a nozzle length of $L_n = 100$ µm, a rise time of the driving wave of 5 µs, and a droplet firing speed of $u = 7$ m/s, which is similar to the flow velocity in the nozzle. The material properties of the ink are roughly $\rho = 1{,}000$ kg/m^3 for the density, $\eta = 10$ mP·s for the dynamic viscosity, $\sigma = 0.05$ N/m for the surface tension, and $\cos\theta \approx 1$ for the cosine of the contact angle. The pressures that have to be overcome to achieve jetting are the dynamic pressure $p_d = \frac{1}{2}\rho u^2$, to overcome inertia; the unsteady pressure $p_i = \rho L_n \mathrm{d}u/\mathrm{d}t$, to accelerate the droplet; the capillary pressure $p_c = 2\sigma\cos\theta/R_n$, which pays for the generated extra surface area; and an extra pressure $p_v = 8\pi\eta L_n u/A_n$, to overcome the viscous resistance of the nozzle. With the above-given material

properties the corresponding values are $p_d \approx 0.25$ bar for the dynamic pressure, $p_i \approx 0.5$ bar for the unsteady pressure, $p_c \approx 0.05$ bar for the capillary pressure, and $p_v \approx 0.7$ bar for the viscous pressure. Together the nozzle pressure must be at least $p_n = p_d + p_i + p_c + p_v \approx 1.5$ bar to allow for jetting at the required velocities. A more general model to estimate the various contributions, based on a momentum balance, was developed by Driessen & Jeurissen (2016).

One of the further advantages of piezoacoustic inkjet printing is that by changing the actuation amplitude, its waveform, and its frequency, the pressure amplitude and, thus, the droplet volume and velocity can be modulated. In general, each channel and therefore each nozzle can be controlled separately. However, one issue that must be taken care of is the so-called cross talk between neighboring channels, meaning that pressure fluctuations in one ink channel are also partially felt in the neighboring ink channel (Wijshoff 2010), given that the distance between neighboring channels should be as small as possible in order to have a compact printhead.

Another huge advantage of piezoacoustic inkjet printing is that the piezoelectric element can be used not only as an actuator but also as an acoustic pressure sensor between the pulses, which allows the acoustics in each individual nozzle to be monitored in detail. This technique is called PAINT (piezoacoustic sensing of ink channels in the time domain) (de Jong et al. 2006b).

CHALLENGE ❷: ENTRAINED BUBBLES IN THE INK CHANNEL

With the PAINT technique, de Jong et al. (2006b) succeeded at finding a correlation between modifications of the pressure response of the ink channel and distortions of the jetting features, namely, a reduction of the droplet jetting velocity. Under certain conditions such distortions can develop after tens of millions of undistorted cycles. de Jong et al. (2006b) identified an air bubble entrained into the ink channel as the reason for both a modified acoustical response and a reduction of the droplet jetting velocity. In the presence of such a bubble, the acoustic pressure building up close to the nozzle is not fully released not only in the droplet jetting but also in the compression of the entrained bubble. Sometimes, after some cycles, the entrained bubble is flushed out together with the drop, but often it grows by rectified diffusion (Brennen 1995, Brenner et al. 2002): For high pressure in the ink channel, the entrained bubble is compressed and loses gas to the surrounding ink, but during the low-pressure period, when the bubble is large, it can gain gas from outside, as the ink contains some dissolved gas. For strong periodic driving, the growth can win. The growing entrained bubble increasingly counteracts the pressure buildup in the channel during the actuation pulse, leading to increasingly lower droplet velocities, until there is a total breakdown of the jetting process (de Jong et al. 2006b, Lohse 2018). In a sense the PAINT method allows one to listen to each ink channel and to hear entrained bubbles, so to speak. It thus also allows one to solve the technological problem of the disturbing bubbles in the ink channel: Once a bubble is detected, the acoustic driving is turned off. During this time other nozzles take over the jetting. The bubble can then fully dissolve, allowing for a reactivation of the nozzle (de Jong et al. 2006b, Wijshoff 2010). Obviously it is much better to avoid the entrainment of bubbles altogether in the first place.

The first evidence of the entrained bubble was thus only indirect, namely, acoustic. Later, de Jong et al. (2006a) and Jeurissen et al. (2009) also succeeded at directly visualizing the entrained bubble by putting a nozzle plate made of glass between the ink channel and the standard metal nozzle plate. By ultrahigh-speed imaging they could reveal the dynamics of the entrained bubbles, both in size and in position. Jeurissen et al. (2008, 2009) and van der Bos et al. (2011a) also developed a model to deduce the bubble size (and thus its growth) from the acoustic sensing signal and successfully compared it with the direct optical visualization of the bubble.

Later, Fraters et al. (2019b) further illuminated the bubble nucleation, translation, and growth with an experimental silicon-based printhead with a glass nozzle plate, using high-speed imaging that was triggered by changes in the ink channel acoustics (i.e., the PAINT signal). An example for the bubble nucleation process in the ink channel is shown in **Figure 4*b***. It can clearly be seen that an impurity in the ink triggers the bubble nucleation upon its interaction with the oscillating meniscus. The inception of cavitation on a dirt particle during the rarefaction pressure wave was identified as a second possible mechanism for the formation of bubbles. Fraters et al. (2019b) even obtained information on how much the entrained bubble reduces the acoustic pressure buildup by employing the entrained bubble as a pressure sensor. They also discovered that the nucleated bubbles translate toward the ink channel walls due to acoustic radiation forces and ink streaming. The vortical flow near the oscillating meniscus was shown to trap impurities, thereby increasing the probability of the particles–meniscus interaction and, correspondingly, of bubble entrainment. In general, the probability of air bubble entrainment increases with increasing driving frequency and with increasing driving pressure (Fraters et al. 2019b). In fact, it is the avoidance of bubble entrainment that is one of the limiting conditions for inkjet printers to operate: Neither the actuation frequency nor the driving pressure must exceed certain thresholds. In the next section on challenge ❸ we see why this is the case.

The above-described optical measurements were conducted with modified ink channels that allowed for optical access. Do such mechanisms also apply to the real MEMS ink channels? With the help of infrared imaging, Fraters et al. (2019a) were able to visualize the dynamics of the bubble entrained in a real technological silicon printhead (which is optically inaccessible). This is possible as the silicon of the printhead is partly transparent to infrared light. These experiments confirmed the above-sketched picture of bubble entrainment and growth by rectified diffusion.

CHALLENGE ❸: FLOW AT THE EDGE OF THE NOZZLE AND ON THE NOZZLE PLATE

Under what conditions does the bubble get into the channel? The probability of an entrainment event at the oscillating meniscus such as that shown in **Figure 4*b*** increases with increasing meniscus oscillation and, thus, with increasing driving pressure and actuation. Moreover, then the meniscus oscillations become more irregular and lose axial symmetry due to a Rayleigh–Taylor instability (van der Meulen et al. 2020). The (initially) exponentially growing meniscus distortions can lead to bubble entrainment as well.

However, an ink film on the nozzle plate can also play a role, with a typical thickness of ~10 nm (de Jong et al. 2007). Its emergence is aided by the inkophilic nature of the nozzle plate. On this film a flow can develop and transport dirt particles toward the meniscus and then distort it, potentially leading to bubble entrainment. This nozzle plate flow can have several possible origins. One is simply air-induced flow due to the jetting of ink. This air flow can drag part of the ink in the film toward the nozzle (see **Figure 5*a***). A concentration gradient in the film can be another origin for such flow, as it induces a Marangoni flow (Scriven & Sternling 1960). Such gradients can develop between neighboring nozzles that jet different inks or due to selective evaporation of one or more components of the ink. The latter case is illustrated in **Figure 5*b***. There, the ink in the nozzle is well mixed, thanks to the acoustic field driving the flow, and therefore has the material properties of the original ink. Further away from the nozzle in the ink film on the nozzle plate or in droplets already sitting on the nozzle plate for longer periods, certain ingredients of the ink have selectively evaporated. This induces a concentration gradient and thus a Marangoni flow along the film–air interface (Beulen et al. 2007, de Jong et al. 2007). Once this flow is directed toward the nozzle, as shown in **Figure 5*b***, it can lead to transport of dirt particles into the nozzle.

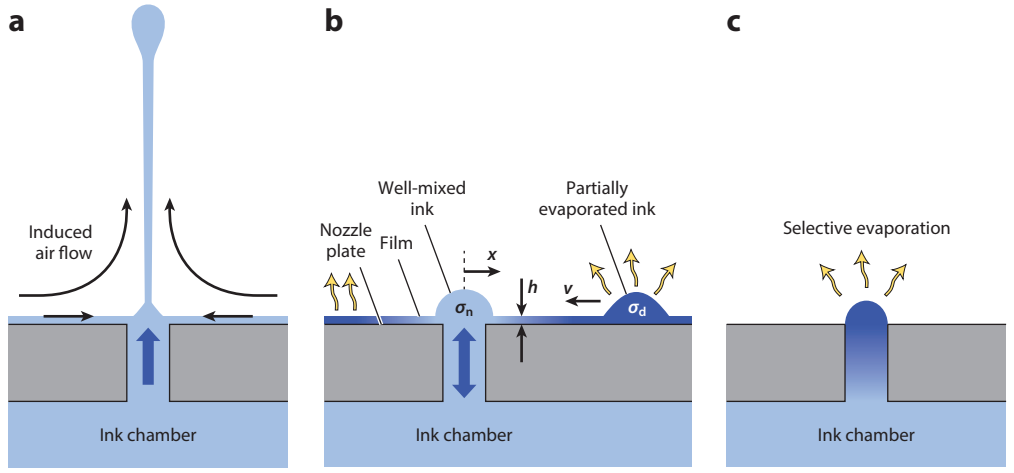

Figure 5

Fluid dynamics on the nozzle plate. (*a*) The jetting of droplets induces an air flow along the jet and also toward the nozzle due to continuity above the surrounding nozzle film, which can partially be dragged along with the air. (*b*) Selective evaporation of one component of the ink induces concentration gradients in the ink film, which has a thickness of about 10 nm (not drawn to scale) on the nozzle plate, leading to Marangoni flows. Here, the high surface tension of the well-mixed ink inside the nozzle leads to a Marangoni force on the ink–air interface, attracting liquid from ink film regions or droplets sitting on the film that have already been subjected to evaporation for some time and have lower surface tension. (*c*) Once a nozzle is at rest for some cycles, partial selective evaporation of one component will lead to a modified surface tension and viscosity at the ink–air interface and, thus, to modified requirements for the pressure pulse to jet the next drop.

Figure 5*b* also shows a droplet on the nozzle plate. Such droplets or ink bands (with a typical thickness of $h \approx 1$–10 μm) on the nozzle plate can occur thanks to the overfilling of the nozzle during the high-pressure phase. They can be many tens of micrometers in diameter and can communicate with the ink in the nozzle thanks to the surface tension difference $\Delta\sigma$ and the resulting Marangoni flow. A simple dimensional analysis gives the scaling relation for the distance $x(t)$ between the droplet on the ink film and the nozzle as (Oron et al. 1997, de Jong et al. 2007)

$$x(t) \sim (h\Delta\sigma/\eta)^{1/2}\,(t_0 - t)^{1/2}; \qquad 1.$$

that is, the droplet velocity $\dot{x}(t) \sim (h\Delta\sigma/\eta)^{1/2}(t_0 - t)^{-1/2}$ diverges with time and the droplet is sucked toward the nozzle with increasing velocity, where it can distort the meniscus oscillations, just as with the dirt particle.

Selective evaporation of one component of a multicomponent ink can cause further problems: Imagine a nozzle at rest for some printing cycles since the particular ink in that nozzle is not needed. In that time—say, many seconds—one or more components of the ink can selectively evaporate out of the nozzle. This changes the material properties of the remaining ink such as the surface tension and the viscosity, and therefore, the required pulse strength for jetting once the nozzle is activated again—a major source of inaccuracy. For example, when the remaining liquid at the meniscus has a higher surface tension or viscosity than the well-mixed ink prior to (partial) evaporation of one or more components, a larger pressure pulse is needed to jet the first droplets after having paused the nozzle, which is clearly an adverse effect for the reproducibility of the jetting process.

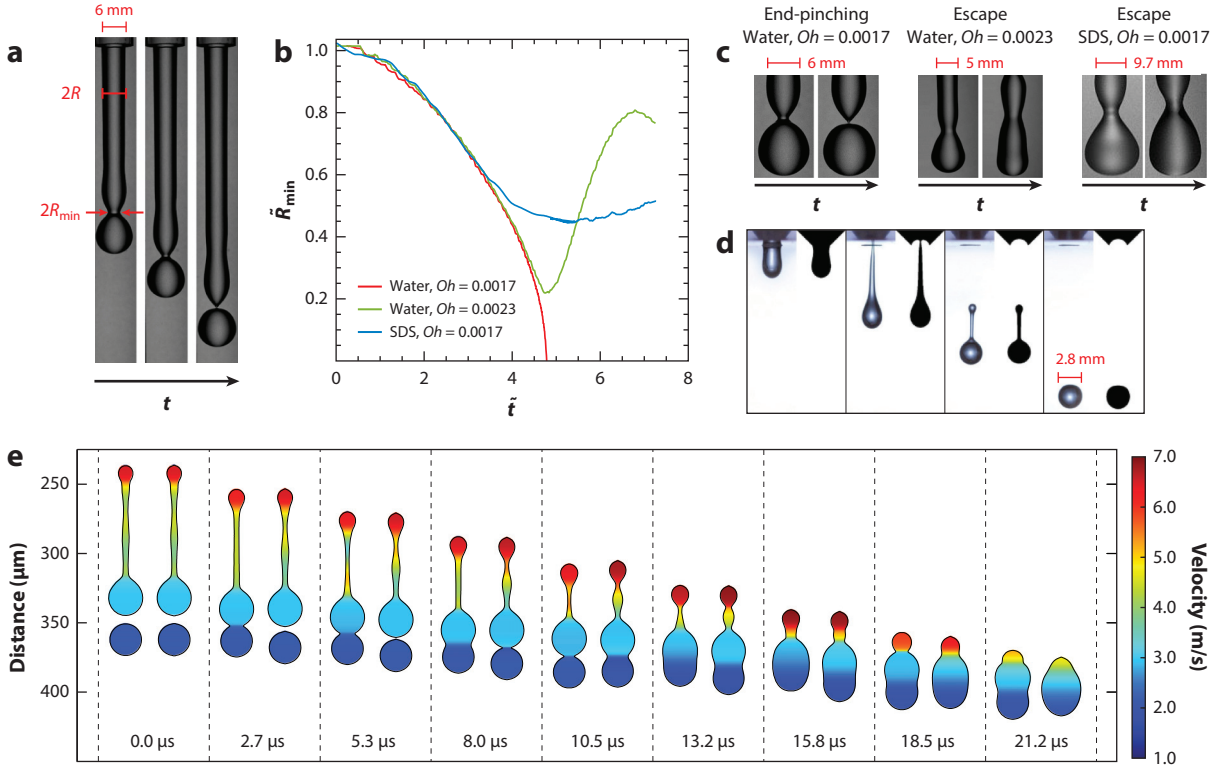

Figure 6

Experimental results on end-pinching and escape from end-pinching. (*a*) Images showing the generation or formation of a filament from a nozzle of diameter $2R$ and the temporal evolution of the filament's shape. The minimal radius of the filament's neck is $R_{\min}(t)$. (*b*) Variation with normalized time $\tilde{t} = t/\sqrt{\rho R^3/\sigma}$ of the normalized minimum filament radius $\tilde{R}_{\min} = R_{\min}/R$ from three experiments: (*red curve*) water, $Oh = 0.0017$; (*green curve*) water, $Oh = 0.0023$; and (*blue curve*) water plus the surfactant SDS (sodium dodecyl sulfate), $Oh = 0.0017$. As also shown by the images depicted in panel *c*, the filament of water of $Oh = 0.0017$ end-pinches, whereas the other two filaments escape from end-pinching. (*c*) Images showing the filaments at two instants in time for the three cases in panel *b*. Panels *a–c* adapted with permission from Kamat et al. (2020). (*d*) Four single-flash images from experiments (*left*) shown alongside the corresponding snapshots from numerical simulations with a finite-element method (*right*), for the same control parameters. Panel *d* adapted with permission from Castrejón-Pita et al. (2011). (*e*) Comparison between the experimental and numerical result for a case of colliding droplets. We show the experimental evolution (*left*) and the numerical results (*right*) at different times. The numerical droplet evolution is calculated from the experimental volume and velocity distributions at $t = 0$ μs. The color scale represents the velocity. Panel *e* adapted with permission from van der Bos et al. (2014).

CHALLENGE ❹: THE JETTING PROCESS, PINCH-OFF, AND SATELLITE FORMATION

For large enough pressure pulses that push the meniscus outward, jetting is finally achieved and the droplet detaches from the ink filament, as seen in **Figures 1** and **6**. The droplet detachment process is also called end-pinching. **Figure 6*a–c*** compares a case in which end-pinching is achieved (red curve in panel *b*) with a case with only slightly higher viscosity [or, in dimensionless form, Ohnesorge number (green curve in panel *b*)] where the droplet escapes from end-pinching (i.e., remains attached to the retracting meniscus; see the second pair of snapshots in **Figure 6*c***). The transition between these two cases corresponds to the transition between the regime of printable fluids (green area in **Figure 3**) to the regime of liquids that are too viscous to print (blue area in **Figure 3**).

The dynamics of the final phase of the end-pinching has been much discussed in the literature: How does the minimal radius $R_{\min}(t)$ approach zero with time? It depends on the regime: For small $Oh \ll 1$, viscosity does not play a role, and from balancing capillary and inertial forces one obtains the famous scaling law (see, e.g., Eggers 1997)

$$R_{\min}(t) \sim (\sigma/\rho)^{1/3}\ (t_0 - t)^{2/3}. \qquad 2.$$

The prefactor in Equation 2 is about 0.7. This capillary pinching of the liquid thread is described by a similarity solution (Eggers 1993, Brenner et al. 1996, Day et al. 1998). For large $Oh \geq 1$, viscous and capillary forces balance and one obtains (Papageorgiou 1995, Eggers 1997)

$$R_{\min}(t) \sim (\sigma/\eta)\ (t_0 - t), \qquad 3.$$

with a prefactor of about 0.071. These two scaling laws for the final phase of the pinch-off are confirmed in various experiments and numerical simulations. In fact, the excellent agreement between experiments and direct numerical simulations holds not only for these scaling laws but also for the full droplet jetting dynamics. An example is shown in **Figure 6*d***, but there are many more in, for example, the papers by Notz & Basaran (2004), Xu & Basaran (2007), Castrejón-Pita et al. (2011, 2012, 2015), Anthony et al. (2019), Antonopoulou et al. (2020), and Kamat et al. (2020).

Moreover, van Hoeve et al. (2010), van der Bos et al. (2014), McIlroy & Harlen (2019), and many others showed that the numerical simulations within the slender jet approximation agree very well with the experiments; van der Bos et al. (2014) achieved such a precision that even the effect of air drag on the droplets could be identified. An example of the good comparison between experiments and numerics in the slender jet approximation is shown in **Figure 6*e***.

In DOD inkjet printing, end-pinching usually is the desired form of droplet formation, but there are other mechanisms, such as droplet formation due to an instability of the filament (the droplet's tail). This can occur when viscosity is too low (i.e., too low Oh) and eventually lead to satellite droplet formation. In **Figure 3** we mark this regime in red, below the red horizontal line $Oh \leq 0.1$, but van Hoeve et al. (2010) have shown by experiments and numerical simulations in the slender jet approximation that satellite droplet may already occur for slightly larger Oh and that the threshold slightly depends on the pulse shape. Similar numerical results have been obtained by Kim et al. (2012) and McIlroy & Harlen (2019) and similar experimental results by Dong et al. (2006) and Liu & Derby (2019), who also have given a nice overview on this subject, including the (weak) dependence of the threshold to satellite droplet formation on the pressure pulse.

As first shown by Shi et al. (1994) and Brenner et al. (1994), the formation of satellite droplets can be hierarchical, with a whole cascade of structures and satellite droplet sizes. Fraters et al. (2020) succeeded at optically resolving four different hierarchies, with primary, secondary, tertiary, and quaternary tails of droplets and satellite droplets down to femtoliters; however, not unexpectedly, the formation of the higher-order tails is irreproducible and therefore presumably controlled by noise.

The competition between satellite droplet formation, end-pinching, and contraction to a single droplet has more systematically and fundamentally been studied in the simpler geometry of a long cylindrical ligament by Stone (1994), Schulkes (1996), Driessen et al. (2013), Anthony et al. (2019), and others. Despite the simplification of the geometry, the outcome is very complicated and various types of ligament breakup scenarios can be achieved. For small initial distortions, a pure breakup through the Rayleigh–Plateau instability can only be achieved for extremely large aspect ratios of the filament, above ∼100 (Anthony et al. 2019). In contrast, Driessen et al. (2014) controlled the jet breakup by exciting and superposing several Rayleigh–Plateau-unstable modes (i.e., by applying large initial distortions of the jet). As summarized by Basaran et al. (2013), next to the filament breakup by the Rayleigh–Plateau instability, in the case of temperature or

concentration gradients the ligament can also break up by a thermocapillary instability or a Marangoni instability, respectively.

Satellite droplet formation in DOD inkjet printing is obviously unwanted. However, it need not be as bad as it seems, as the satellite droplets may get recollected again by the main droplets. One example by van der Bos et al. (2014) for the collision between the main droplet with the satellite droplet—both in experiments and in the nicely agreeing corresponding numerical simulations in the slender-jet approximations—is shown in **Figure 6*e***. Similar examples are given in the numerical work of McIlroy & Harlen (2019), who identify the conditions under which the satellite droplets can merge again with the main drops. Obviously, these strategies will fail once the satellite droplets are so small (for small enough Stokes number *St*) that they experience lateral air drag forces and drift away from the jetting axis. Then they are a source of contamination.

How then to delay the formation of satellite droplets and extend the regime of printable fluids (green area in **Figure 3**) toward smaller Ohnesorge numbers? One strategy is to fine-tune the time variation of the pressure pulse (Dong et al. 2006, Fraters et al. 2020). A more drastic strategy is to add surfactants (Kamat et al. 2018, 2020; Manikantan & Squires 2020) or use non-Newtonian inks with some elasticity (Tirtaatmadja et al. 2006, Ardekani et al. 2010, Bhat et al. 2010, Hoath et al. 2012, Keshavarz et al. 2015), characterized by a nonzero Deborah number *De*. One example is given in **Figure 6*b*,*c***, taken from Kamat et al. (2020), where the addition of a small amount of the surfactant SDS (sodium dodecyl sulfate) suppresses even the end-pinching for otherwise unchanged control parameters *Oh* and *Re*. The addition of surfactants or of liquid that allows for some yield-stress can also considerably change the scaling laws (Equations 2 and 3) of the end-pinching (Louvet et al. 2014, Wee et al. 2020).

A final aspect of the droplet's travel between the nozzle and the substrate is connected with the droplet's shape oscillation: Since at pinch-off elongational forces are exerted on the droplet, after pinch-off the free droplets undergo shape oscillations whose frequencies (Rayleigh frequency) are set by the surface tension and whose damping is set by the liquid viscosity (Lamb 1932) or, in dimensionless form, the capillary number *Ca*. Such shape oscillations have been visualized (Staat et al. 2017) and numerically modeled (Basaran 1992, Wang et al. 2019). As this latter paper shows, the deformation strongly and nonmonotonically depends on *Ca*, with a maximum around $Ca = 0.7–0.8$. Obviously, whether the droplet is elongated in the axial direction or compressed at the moment of impact matters for the droplet's spreading behavior on the receiving substrate.

CHALLENGE ❺: DROP IMPACT, SPREADING, AND SPLASHING

Apart from the droplet's shape at the moment of impact, this spreading behavior is again determined by the Reynolds number and the Weber number (or Ohnesorge number) of the droplet (see **Figure 3**). In addition, there are many other parameters that influence drop impact. Namely, the spreading and splashing are strongly affected by the advancing contact angle between the liquid and the substrate, the type and roughness of the targeted substrate (Quéré 2008; Xu 2007; Xu, Barcos & Nagel 2007; Tsai et al. 2011), the impact angle (Mundo et al. 1995), the temperature of the substrate (Tran et al. 2012, Quéré 2013), and even the ambient air pressure (Qian & Law 1997, Xu et al. 2005, Driscoll et al. 2010, Tsai et al. 2010), reflected in the Stokes number *St* of the droplet at impact.

The reason for the relevance of the ambient air is that just before impact the air between the drop and the receiving substrate is compressed. This pressure buildup leads to a deformation of the drop, namely, a dimple formation (Thoroddsen et al. 2005, Hicks & Purvis 2010, Driscoll & Nagel 2011, Bouwhuis et al. 2012, Kolinski et al. 2012, Mandre & Brenner 2012) (see **Figure 7*a***). In the early phase of the impact, the droplet is floating on air, so to speak. In fact, as Mani et al. (2010)

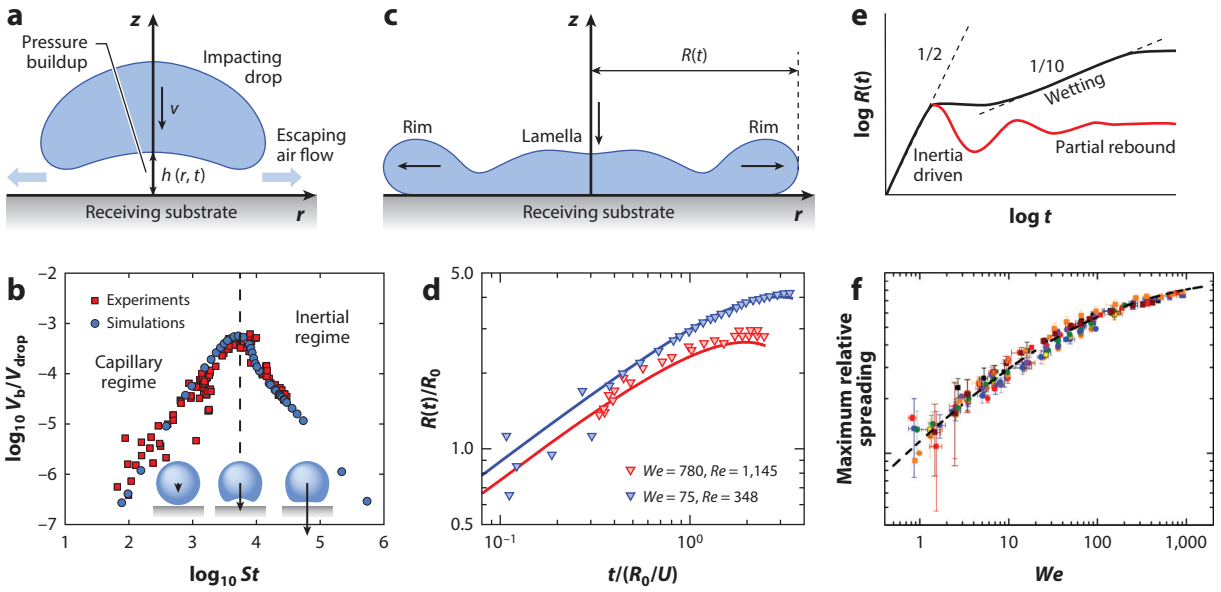

Figure 7

The droplet during impact, spreading, and wetting, along with corresponding data. (*a*) The droplet just prior to impact: The pressure buildup under the droplet leads to a droplet deformation, and an air cushion forms between the impacting droplet and the receiving substrate. (*b*) The relative volume of the entrained bubble V_b/V_{drop} as function of the Stokes number St. Red squares are from experiments, and blue circles are from numerical simulations. Panel *b* adapted with permission from Bouwhuis et al. (2012). (*c*) After contact, the droplet radially spreads and a rim forms at the edge of the spreading drop, which can undergo a Rayleigh–Plateau instability (not shown). Depending on the liquid and substrate properties, the droplet then either recoils or further wets the substrate thanks to an advancing contact line. (*d*) Relative spreading $R(t)/R_0$ for two different combinations of the Weber number We and Reynolds number Re. The symbols are experimental data from Visser et al. (2015), and the solid lines are from the theory of Gordillo et al. (2019). (*e*) Sketch of the contact radius $R(t)$ for two scenarios: partial rebound and further wetting. (*f*) Universality of the maximum droplet relative spreading radius $[(R_m/R_0)^2 - (R_m(U \to 0)/R_0)^2]^{1/2}$ after impact according to Equation 4 for various viscosities and liquids (marked by different colors), as well as smooth (*squares*) and rough (*circles*) surfaces. Panel *f* adapted with permission from Lee et al. (2016).

and Mandre & Brenner (2012) have shown, air is pushed out from the region between the droplet and the substrate, and this air flow interacts with the droplet itself, which can lead to splashing (Xu et al. 2005, Riboux & Gordillo 2014). Eventually, after touchdown, the dimple formation at the bottom side of the droplet leads to the entrapment of an air bubble under the droplet (van Dam & Clerc 2004, Thoroddsen et al. 2005, Bouwhuis et al. 2012, Lin et al. 2018). The relative volume of this entrained bubble as compared to the volume of the droplet itself happens to be maximal at the typical parameters occurring at drop impact in piezoacoustic inkjet printing. Taking again a droplet diameter of 20 μm, a velocity of 10 m/s, and ambient conditions, the corresponding Stokes number is about $St = 8{,}000$, very close to the maximal value of the relative volume V_b/V_{drop} (Bouwhuis et al. 2012) (see **Figure 7*b***). For larger impact velocities (or St), inertia dominates and the effect of the air on the deformation of the droplet fades away, whereas for smaller velocities (or St), capillarity takes over so that the droplet deformation through the air is counteracted, and the entrained bubble is small as well. As Bouwhuis et al. (2012) showed, balancing the respective forces in these two regimes results in the scaling laws $V_b/V_{drop} \sim St$ and $V_b/V_{drop} \propto St^{-4/3}$ for the relative bubble volume for small and large St, respectively.

In inkjet printing, the flow of the escaping air prior to impact, the dimple formation, and the resulting air bubble entrainment under the impacting droplet are unwanted effects, as the air flow enhances splashing and the bubble entrainment can lead to modified optical properties of the drop and reduce the direct contact between drop and receiving substrate.

After touchdown, in the second phase of the impact, the ink radially spreads outward, driven by inertia (**Figure 7*c***). In the beginning of this spreading process the radius $R_n(t)$ of the touching area obeys Wagner's theorem, $R_n(t) = \sqrt{3R_0Ut}$ (Riboux & Gordillo 2014), in nice agreement with various experiments and numerical simulations over a large parameter range [see, e.g., Gordillo et al. (2019) and **Figure 7*d***]. Later capillary forces counteract this spreading, pulling back the ink and leading to a rim formation at the edge (Eggers et al. 2010, Wildeman et al. 2016, Gordillo et al. 2019) (see **Figure 7*c***). Additionally, viscous dissipation counteracts the spreading and, for small Reynolds numbers, can even be dominant (Wildeman et al. 2016). During contraction, the receding contact angle plays a role as well. The impacting droplet can also partially bounce in an oscillatory way (Josserand & Thoroddsen 2016, Lin et al. 2018) (see the sketch in **Figure 7*e***).

The balance between inertial forces, on the one hand, and capillarity and viscous forces, on the other hand, determines the maximal radius $R_m = \max_t[R_n(t)]$ of the spreading. As described by Josserand & Thoroddsen (2016), various models have been suggested for the dependence $R_m/R_0 = f(Re, We)$ over the years. Here, we give the model by Laan et al. (2014) and Lee et al. (2016),

$$\left[\left(\frac{R_m}{R_0}\right)^2 - \left(\frac{R_m(U \to 0)}{R_0}\right)^2\right]^{1/2} = \frac{Re^{1/5}We^{1/2}}{A + We^{1/2}}, \qquad 4.$$

which is based on an interpolation between the capillarity-dominated regime (for small We, with $R_m/R_0 \propto We^{1/2}$) and the viscosity-dominated regime (for small Re, with $R_m/R_0 \propto Re^{1/5}$). Here $R_m(U \to 0)$ is the maximal radius of a gently deposited droplet. The model has one free parameter, $A = 7.6$, which is obtained from a fit to the experimental data. As seen from **Figure 7*f***, these are then well described over a large parameter range in the Re versus We parameter space. We also refer the reader to Gordillo et al. (2019) for approximate analytical expressions for $R(t)$ and $R_m(We, Re)$, which are based on mass and momentum balances.

For large enough impact velocity, the spreading rim can destabilize, either by a Rayleigh–Plateau instability (Zhang et al. 2010, Agbaglah et al. 2013) or by splashing (Xu et al. 2005, Riboux & Gordillo 2014, Josserand & Thoroddsen 2016); both mechanisms break the axial symmetry of the process. For the latter the escaping air flow plays a central role. Riboux & Gordillo (2014) worked out a predictive model for the onset of this splashing behavior. The splashing can also be triggered by some roughness of the receiving substrate (Josserand & Thoroddsen 2016).

In the long term, wetting effects can play a role (Bonn et al. 2009), provided the contact angle is small enough, for example, for ethanol droplets on glass (de Goede et al. 2019) or for silicon oil (Tanner 1979). In that regime, Tanner's law $R(t) \sim t^{1/10}$ holds (Tanner 1979, Kant et al. 2017) [see Bonn et al. (2009) and the sketch in **Figure 7*e***]. Finally, we note that surfactants can also modify the drop impact dynamics (Zhang & Basaran 1997).

CHALLENGE ❻: DROP COALESCENCE, DROP–FILM INTERACTION, AND INK INTRUSION INTO PAPER

After impact, the jetted droplets can interact through capillary effects. Our understanding of the merging (or coalescence) of sessile drops of pure and identical fluids (**Figure 8*a***) has become more detailed in recent years (Ristenpart et al. 2006, Kapur & Gaskell 2007, Lee et al. 2012, Eddi et al. 2013, Sui et al. 2013). As compared to the coalescence of freely suspended droplets in

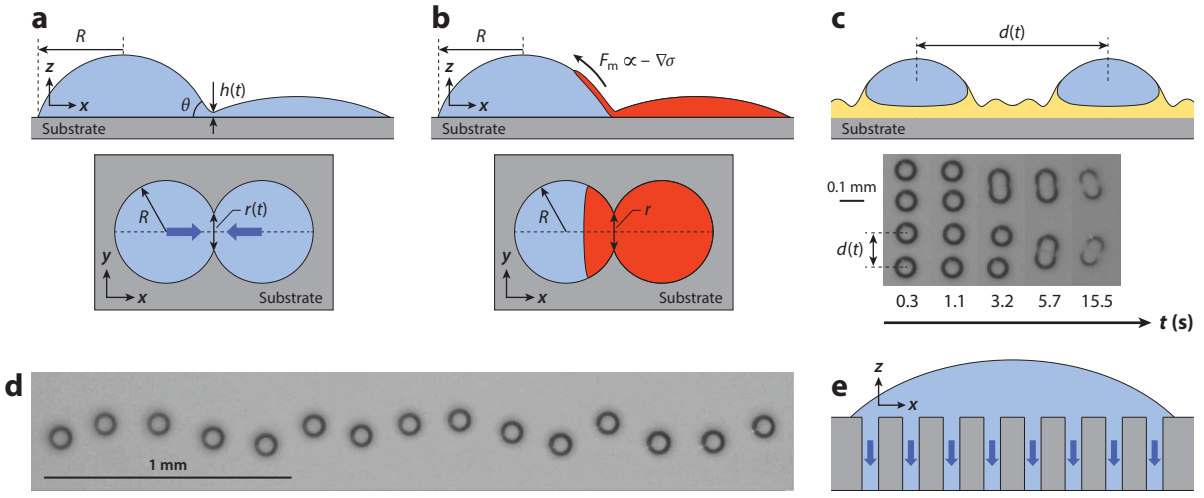

Figure 8

(*a*) Merging of two neighboring droplets on the receiving substrate after contact due to capillary forces: side view (*top*) and top view (*bottom*). (*b*) In contrast, for two drops of different liquids with different surface tensions, the one with the lower surface tension can creep over the other due to Marangoni forces: side view (*top*) and top view (*bottom*). (*c*) Two droplets on a thin viscous film can attract or repel each other due to capillary forces, mediated by a visco-capillary wave on the thin film and induced by the droplets themselves: side view (*top*) and a top view of an experimental realization for attraction (Hack et al. 2018) (*bottom*). (*d*) Self-arrangement by mutual repulsion of droplets originally printed in a row on a thin liquid film. The only difference with respect to panel *c* is the initial distance between the droplets. Panels *c* (*bottom*) and *d* adapted with permission from Hack et al. (2018). (*e*) Schematic of the ink entrainment process into a porous substrate. Panel *e* adapted with permission from Pham & Kumar (2019).

air, where the width of the neck scales as $r(t) \sim (\sigma/\eta)t \log[\sigma t/(\eta R)]$ in the viscous regime or as $r(t) \sim (\sigma R/\rho)^{1/4} t^{1/2}$ in the inertial regime (Eggers et al. 1999, Duchemin et al. 2003, Paulsen et al. 2011, Sambath et al. 2019, Anthony et al. 2020), for sessile drops the main complication is due to the presence of the substrate, which introduces additional interactions that come with the complexities associated to the spreading and pinning of contact lines (Bonn et al. 2009, Snoeijer & Andreotti 2013). Considering these, Ristenpart et al. (2006), Hernandez-Sanchez et al. (2012), and Eddi et al. (2013) obtained the scaling of the height $h(t)$ of the bridge between the two droplets for the viscous and inertial regimes, respectively (see **Figure 8*a***):

$$h(t) \sim \theta^4 \sigma \eta^{-1} t \quad \text{and} \quad h(t) \sim f(\theta) \sigma^{1/3} \rho^{-1/3} t^{2/3}. \qquad 5.$$

In the viscous regime, which is the more relevant here, the width of the bridge now scales differently, namely as $r(t) \sim \sqrt{Rh(t)/\theta} \sim \theta^{3/2} R^{1/2} \sigma^{1/2} \eta^{-1/2} t^{1/2}$.

In **Figure 8*b*** the coalescence of two droplets, consisting of different inks, is sketched. Though of obvious practical relevance, in this case our understanding of the detailed coalescence dynamics is far from complete. In the case of coalescence of different but fully miscible droplets, a large enough surface tension difference at the interface (i.e., a large enough Marangoni number) will lead to Marangoni flow, with the droplet of smaller surface tension liquid being pulled over that with the larger one (Karpitschka & Riegler 2010), while the counteracting force in general is of viscous nature. Such Marangoni flows can lead to unwanted effects, particularly if they transport pigments, thus affecting the achievable resolution and color fidelity. In other cases the emerging Marangoni flow between the droplets can help with mixing the droplets (bleeding of mixed colors) (see, e.g., Sykes et al. 2020). For smaller Marangoni numbers below a certain threshold Karpitschka & Riegler (2012, 2014) and Sykes et al. (2020) showed that the coalescence between the droplets

can also be delayed, due to a competition between capillary pressure and dynamic pressure induced by the Marangoni flow.

Cira et al. (2015) demonstrated that the interaction between neighboring droplets can even occur when they are not touching each other, namely, through the ambient air by evaporation-induced surface tension gradients. Thus, droplets can move in response to the vapor emitted by their neighbors. Once droplets consisting of different liquids get in contact with each other, they can also react (Jehannin et al. 2015). Then the crucial new parameter entering the game is the Damköhler number *Da*, which compares the timescale of the chemical reaction with that of the hydrodynamics.

In inkjet applications the ink often is deposited not on a dry substrate, but on a thin viscous primer film consisting of (coalesced) prior droplets or a coating layer placed prior to the actual printing process (see **Figure 8*c***). Then just prior to drop impact, both the droplet itself and the thin film get deformed due to the air-cushioning effect (Hicks & Purvis 2011, Pack et al. 2017, Tang et al. 2019), and additionally, waves can emerge on the thin film. As Motaghian et al. (2019) showed, surface tension differences between the droplet and the film can also lead to rapid spreading of droplet on the film, jeopardizing precise droplet deposition.

Two drops placed close together on such a thin viscous film can interact via deformations of the film: Hack et al. (2018) showed that the interaction can be either attractive or repulsive, depending on the distance separating the two drops. The distance at which the interaction changes from attraction to repulsion was found to depend on the thickness of the film and increase over time. Hack et al. (2018) revealed that the origin of the nonmonotonic interactions lies in the appearance of a visco-capillary wave on the thin film, which is induced by the drops. Using the thin-film equation, they identified the scaling law for the spreading of the waves and demonstrated that this governs the range over which the interaction is observed. A top view of the self-arrangement of the droplets printed on the viscous film is shown in **Figure 8*d***, demonstrating that printing straight lines on thin films can be challenging. This even holds for printed lines on dry substrates, as Duineveld (2003) has shown.

Finally, the deposited ink droplet can also be absorbed into the substrate, provided it is porous, such as paper (Gambaryan-Roisman 2014) (see the schematic sketch in **Figure 8*e***). The timescale of absorption is one of the key parameters that determines the maximum achievable printing speed. The liquid ink can also result in an expansion of the porous substrates, leading to undesirable instabilities such as waviness, curling, and cockling.

CHALLENGE ❼: EVAPORATION AND SOLIDIFICATION OF THE INK

The final stage of a droplet is its drying or solidification process, the latter happening either by cooling or by chemical reactions, such as cross-linking of different ingredients of the ink.

The evaporation of an isolated sessile pure liquid droplet in volumes down to microliters is today quite well understood. However, this is much less the case for the evaporation of picoliter colloidal droplets, which are the relevant ones in inkjet printing. Although the evaporation of picoliter droplets will be governed by the diffusion of the vapor in the surrounding air, just as for microliter droplets, differences may occur due to pinning/depinning effects on the surface (de Gennes 1985, Bonn et al. 2009, Lohse & Zhang 2015) because, for picoliter droplets, the separation between the length scales of typical surface inhomogeneities and those of the droplet itself is much less pronounced. Correspondingly, depending on the type of surface and the suspended pigments, the droplet may evaporate in various different modes (Picknett & Bexon 1977, Stauber et al. 2014, Zhang et al. 2015), such as the constant–contact radius (CR) mode, the constant–contact angle (CA) mode, the stick–slip mode, or the stick–jump mode (Lohse & Zhang 2015). At

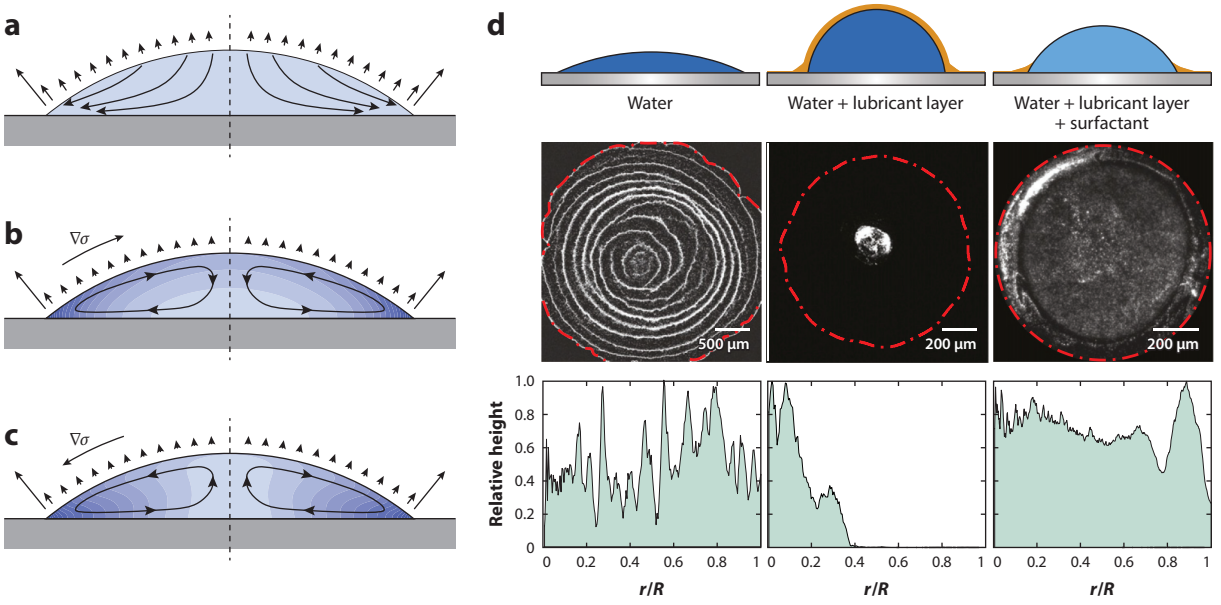

Figure 9

Evaporation of different types of colloidal droplets with a pinned contact line. The lengths of the radially outward arrows show the local evaporation rate, which is controlled by the vapor diffusion outside the droplet. In all cases the contact lines are pinned (i.e., evaporation takes place in the constant–contact radius mode). (*a*) Pure liquid colloidal droplet, as in Deegan et al. (1997), leading to the coffee stain effect. (*b*) Binary colloidal liquid, where the more volatile liquid has the higher surface tension. Correspondingly, at the droplet–air interface the flow goes inward toward the apex. Mean relative concentration of the less volatile liquid is indicated by darker shading. An example would be a mixture of water (more volatile, larger σ) and glycerol. (*c*) Binary colloidal liquid, where the more volatile liquid has the lower surface tension. Correspondingly, at the droplet–air interface the flow goes outward toward the rim. An example would be a mixture of ethanol (more volatile, smaller σ) and water. (*d*) Evaporating sessile colloidal droplets on a substrate under different conditions: (*left column*) a colloidal water droplet on a dry substrate, (*middle column*) a colloidal water droplet on a lubricated surface, and (*right column*) a colloidal water droplet seeded with the surfactant SDS (sodium dodecyl sulfate). (*Top row*) Schematic drawings. (*Middle row*) Comparison of the final deposition patterns after full evaporation of the droplets in these three cases; the red dashed lines indicate the original contact line positions. (*Bottom row*) Respective deposition profiles along the radius from the center to the original droplet edge. In the first column, ring formation is seen due to the stick–slip evaporation mode. In the second column, the deposition is only at the center of the droplet. In the third column, it is more or less homogeneous. Figure adapted with permission from Li et al. (2020a).

first sight, a pure CR mode may seem to be the most desirable one for inkjet printing, as the full initial contact area remains wetted up to the very end. However, for colloidal droplets consisting of a pure liquid, evaporation in the CR mode often implies ring formation of the deposit—the notorious coffee stain effect (Deegan et al. 1997, Marin et al. 2011, Kaplan & Mahadevan 2015), occurring in the final stage of the droplet drying process. The mechanism of the coffee stain effect is illustrated in **Figure 9*a***: Due to the geometric singularity at the rim, the evaporation rate is highest there, transporting the liquid there. It takes along the colloid particles, which get stuck there, forming a ring-like deposit. Obviously, in printing applications such stain formations are highly undesirable.

How to overcome the coffee stain effect in inkjet printing applications? The answer lies in the composition of the ink, which usually does not consist of a pure liquid but is designed as a highly sophisticated mixture of multiple components, also containing surfactants. This complex composition of the ink has a huge impact on the drying process: Due to the different volatilities, selective evaporation may occur, leading to concentration gradients and thus Marangoni

forces along the droplet–air interface. These induce flows inside the droplet (Scriven & Sternling 1960; Hu & Larson 2005; Christy et al. 2011; Bennacer & Sefiane 2014; Kim et al. 2016, 2017; Tan et al. 2016; Diddens et al. 2017b; Karpitschka et al. 2017; Edwards et al. 2018; Kim & Stone 2018; Li et al. 2018, 2019a; Marin et al. 2019), with all their consequences for the pigment distribution on the substrate. Two examples for binary droplet evaporation in the CR mode are shown in **Figure 9*b*,*c***, with different relations between the relative volatilities and surface tensions, leading to flows in opposite directions and correspondingly to different deposition and coating patterns (Cai & Zhang-Newby 2008, Han & Lin 2012, Kuang et al. 2014, Sefiane 2014, Kim et al. 2016). For the case of **Figure 9*b***, the inward-pointing Marangoni forces can imply a so-called Marangoni contraction, with an effective contact angle larger than expected from the Young–Laplace equation (Karpitschka et al. 2017).

The strength of the Marangoni flow can vary over a large range. For large Marangoni numbers *Ma* it can be so violent—with velocities exceeding millimeters per second—that the axial symmetry breaks (Kim et al. 2016, Diddens et al. 2017b). In contrast, for small *Ma* it can be so weak that the liquid mixes insufficiently. Consequently, the selective evaporation of one liquid can lead to segregation of this liquid in the center of the droplet thanks to shielding by the other, nonvolatile liquid (Karpitschka 2018, Kim & Stone 2018, Li et al. 2018).

The dynamics of evaporating binary sessile droplets is further complicated once surfactants also come into play (Kim et al. 2016, 2017; Marin et al. 2016; Bruning et al. 2018; Li et al. 2020b; van Gaalen et al. 2021). These and the composition of the binary droplet strongly affect the pattern of the deposit, as Kim et al. (2016) demonstrated with evaporating whisky droplets. By combining surfactants with a lubricant oil layer, Li et al. (2020a) could even fully suppress the coffee stain formation (see **Figure 9*d***).

A plethora of further phenomena can emerge for evaporating droplets: Ristenpart et al. (2007) showed that thermal effects connected with the thermal conductivity of the substrate can invert the internal flow in the evaporating droplet and thus strongly affect the deposition pattern, with thermal Marangoni forces playing a crucial role. Additionally, Talbot et al. (2012) and Schofield et al. (2018) worked out the influence of thermal effects on the lifetime of the droplets and showed that they can significantly extend it. Marin et al. (2019) revealed that the solutal Marangoni stresses originating from dissolved salts also strongly affect the internal flow in the droplet and thus the emerging stain pattern. Wang et al. (2021) added different concentrations of hygroscopic salts to the droplet and could thus tune its vapor adhesive versus evaporative properties, revealing rich and diverse flow dynamics according to the competition between capillary and thermal and solutal Marangoni forces. Williams et al. (2021) experimentally and theoretically studied the spreading and retraction of an evaporating sessile droplet of a volatile binary mixture on a substrate with high wettability (i.e, with a precursor layer), as well as how this depends on the various control parameters, including thermal effects.

For droplet evaporation on a porous substrate such as paper the remaining deposit tends to be more homogeneous, as infiltration of the colloidal liquid into the pores can win over particle motion (Dou & Derby 2012, Boulogne et al. 2015, Pack et al. 2015, Pham & Kumar 2019), giving an opportunity to overcome the coffee stain effect, namely, when the combined effect of infiltration and evaporation is faster than the timescale of advective and diffusive particle transport.

Finally, we mention that the evaporation of an isolated sessile droplet is of course the exception in inkjet printing applications, where many droplets are closely placed on the receiving substrate so that their evaporation processes affect each other, generally delaying evaporation due to mutual shielding effects. This also affects the deposition pattern deposit each droplet leaves (Schäfle et al. 1999, Wray et al. 2020).

As already mentioned, beyond evaporation and droplet drying, other means of droplet solidification have become increasingly important in DOD inkjet printing. For hot melt inks, this involves solidification by cooling below their freezing temperatures and crystallization. Obviously, the heat exchange with the substrate is of prime importance, as the spreading of the solidifying drop is arrested when the liquid at the contact line falls below a critical temperature (de Ruiter et al. 2017, Jalaal et al. 2018). In other cases the solidification is achieved by UV radiation triggering polymerization or by chemical cross-linkers, which are brought into contact with a droplet after deposition, leading to solidification (Visser et al. 2018). Many further cases of droplet solidification of complex fluids droplets, including emerging mechanical instabilities such as buckling, are discussed by Giorgiutti-Dauphiné & Pauchard (2018).

OUTLOOK, CHALLENGES, AND OPEN QUESTIONS

As empirical evidence over the last 40 years has shown, Moore's law holds not only for the semiconductor industry but also for inkjet printing: The droplet jetting frequency per printhead grows exponentially, roughly doubling every two years. In 1984 it was at 10^7 drops per second from all nozzles of a printhead, going up to 10^{11} drops in 2020. We would like to stress that this is not a law of nature but has required tremendous research and development efforts, and it will continue to require these—if Moore's law is supposed to be continued. In this final section we outline some of the specific and, in particular, new fundamental fluid dynamics challenges that the community has to confront in coming years in order to continue to be able to follow Moore's law in DOD inkjet printing.

Faster and More Stable Drop-on-Demand Inkjet Printing

In order to proceed toward faster inkjet printers with even smaller droplets, we need further quantitative understanding of the effect of the entrained bubbles on the acoustic field in the channel and therefore on the droplet formation process. Moreover, we must find ways either to avoid air entrainment or to get rid of the bubble faster than its passive dissolving, e.g., by applying some kind of recovery pulse to the piezo actuator in an early phase after bubble entrainment.

To achieve this, one must better understand the fluid dynamics within the printhead, including the acoustics and the wetting properties at the nozzle, the droplet formation process, and the droplet dynamics at the nozzle. This includes the actuation principles and performance, acoustic ink channel modeling, mixing processes in the ink channel, the meniscus dynamics, air bubble entrainment, and the wetting properties of the nozzle plate and its coatings.

However, to resolve the complicated meniscus dynamics and the dynamics of the entrained bubble, it is clearly necessary to go beyond optical ultrahigh-speed imaging, toward imaging techniques beyond the optical regime. Here, high-speed imaging with X-rays, following the pioneering work of Agbaglah & Deegan (2014) and Agbaglah et al. (2015), offers an opportunity. With this technique, it will be possible to image at length scales two orders of magnitude smaller that optical imaging, thus allowing for the detection of bubble nuclei in the ink channel at a very early stage.

Colloidal Interaction

Many of the new challenges in piezoacoustic inkjet printing are due to the specific physicochemical challenges of the multicomponent and multiphase nature of the ink. This holds in particular for latex inks, which contain pigments as colloidal particles, with volume fractions of 10–20% and particle diameters between 10 nm and 10 μm. For the smaller particles, the van der Waals

attraction is crucial, which can lead to aggregation and clogging. Its strength depends on the salt concentration and can thus be tuned. Salt can be added not only to the ink itself but also through a prelayer of a thin salty liquid or through salt crystals on the substrate. The repelling force between the particles is due to steric stabilization by polymers or due to electrostatic interaction—these too can be tuned. Both have a bearing on the ink behavior in the nozzle (clogging), on the nozzle plate, and on the substrate (patterns like the coffee stain) and need fine-tuning, which must be based on a thorough theoretical understanding, and not on trial-and-error. Presently, this understanding is missing. A key question to address is: How is the droplet spreading affected by the presence of the salt on the substrate, both from a mechanical and from a chemical point of view?

Film Formation by Evaporation

The jetted droplets eventually must form a film. For aqueous inks, with no organics involved, this is simply achieved by evaporation: The pigments stay behind. For optimal quality of the print, namely, a homogeneous film, droplet coalescence is essential. This holds on a short timescale of milliseconds, but also on long timescales, as the drying process can take up to hours and even days, as interdiffusion is a very slow process. It can be affected by surfactants, the chemical composition of the ink's carrier liquid, the particle size, their steric stabilization, and even cross-linking, but also by the surface roughness, its porosity, and environmental conditions such as temperature and humidity.

Surfactants

Surfactants deserve their own subsection or item in the list of open problems. Manikantan & Squires (2020) call surfactants the "hidden variables controlling fluid flows," and in DOD inkjet printing they can play an essential role throughout the inkjet printing process, from the nozzle plate flow to the droplet jetting and satellite formation, the impact, droplet–droplet and droplet–film interactions, and drying (i.e., challenges ❸ through ❼). The variety of surfactants is huge and our quantitative understanding of their impact on the fluid dynamics of DOD inkjet printing is in its infancy.

Chemical Drying of Neighboring Droplets

What exactly happens when one reactant diffuses into a droplet of another reactant (e.g., from a neighboring droplet or from some reservoir)? How does the reaction propagate from the droplet surface where the two reactants first make contact? How does a two-component paint chemically dry through cross-linkers? Watching paint dry is in fact an interesting, relevant, and largely unexplored science!

Film Formation by Polymerization by Ultraviolet Radiation

Nonaqueous inks, which contain organic liquids, are solidified by polymerization, often initialized by UV radiation. The emerging films are more robust and used for outside applications. The challenges are the same as for the film formation through evaporation in aqueous inks: The film should be homogeneous. The UV radiation triggers a chemical reaction, often through cross-linkers. With the timescale of the polymerization (i.e., with the intensity of the UV light), the appearance of the film can be tuned: Once it is faster than the timescale of the droplet coalescence, the film structure appears to be matte and the hilly structure of the original droplets is frozen in.

Vice versa, once the curing timescale of the polymerization is slow, the droplets can fully coalesce and equilibrate, and the appearance of the film is glossy. However, a quantitative understanding of this competition process is still to be developed.

Multicomponent Droplet Evaporation Under an Air Flow

In industrial piezoacoustic inkjet printing, the multicomponent droplet evaporation takes place not in still air, but under an air flow. This holds both for the nozzle side and for the paper side: Obviously, air flow emerging from the paper that is processed will considerably enhance the droplet evaporation. The new parameter entering is the Péclet number, given by the velocity of the paper passing by the nozzle. Evaporation that is too fast on the nozzle side can have serious consequences, such as ink drying in nozzles. This will block further jetting activity and thus must be avoided.

DISCLOSURE STATEMENT

Over the last 20 years, the author has received various research grants jointly financed by Océ (now Canon) and the Dutch Research Council (NWO).

ACKNOWLEDGMENTS

We thank all colleagues, postdocs, PhD students, and undergraduate students for all their work and contributions to our understanding of the inkjet printing process with its various and rich aspects and for the stimulation and intellectual pleasure we have enjoyed when doing physics together on this great subject. In particular, we thank Christian Diddens, Hans Reinten, Tim Segers, Jacco Snoeijer, Marc van den Berg, Michel Versluis, and Herman Wijshoff for nearly two decades of collaboration. Moreover, we thank these individuals along with Osman Basaran, José Gordillo, John Hinch, Alvaro Marin, Andrea Prosperetti, and Howard Stone for comments on the manuscript and Dennis van Gils for drawing the figures. This work is part of an Industrial Partnership Programme (IPP) of NWO. This research program is cofinanced by Canon Production Printing Holding B.V., University of Twente, and Eindhoven University of Technology. We also gratefully acknowledge support by the ERC Advanced Grant DDD (project number 740479) and by the Max-Planck-Center Twente, which is cofinanced by NWO.

LITERATURE CITED

Agbaglah G, Deegan RD. 2014. Growth and instability of the liquid rim in the crown splash regime. *J. Fluid Mech.* 752:485–96

Agbaglah G, Josserand C, Zaleski S. 2013. Longitudinal instability of a liquid rim. *Phys. Fluids* 25(2):022103

Agbaglah G, Thoraval MJ, Thoroddsen ST, Zhang LV, Fezzaa K, Deegan RD. 2015. Drop impact into a deep pool: vortex shedding and jet formation. *J. Fluid Mech.* 764:R1

Aidun CK, Clausen JR. 2010. Lattice-Boltzmann method for complex flows. *Annu. Rev. Fluid Mech.* 42:439–72

Ambravaneswaran B, Wilkes ED, Basaran OA. 2002. Drop formation from a capillary tube: comparison of one-dimensional and two-dimensional analyses and occurrence of satellite drops. *Phys. Fluids* 14(8):2606–21

Anthony CR, Harris MT, Basaran OA. 2020. Initial regime of drop coalescence. *Phys. Rev. Fluids* 5(3):033608

Anthony CR, Kamat PM, Harris MT, Basaran OA. 2019. Dynamics of contracting filaments. *Phys. Rev. Fluids* 4(9):093601

Antobe BV, Wallace DB. 2002. Acoustic phenomena in a demand mode piezoelectric ink jet printer. *J. Imaging Sci. Technol.* 46:409–14

Antonopoulou E, Harlen O, Walkley M, Kapur N. 2020. Jetting behavior in drop-on-demand printing: laboratory experiments and numerical simulations. *Phys. Rev. Fluids* 5(4):043603
Ardekani A, Sharma V, McKinley G. 2010. Dynamics of bead formation, filament thinning and breakup in weakly viscoelastic jets. *J. Fluid Mech.* 665:46–56
Basaran OA. 1992. Nonlinear oscillations of viscous liquid drops. *J. Fluid Mech.* 241:169–98
Basaran OA. 2002. Small-scale free surface flows with breakup: drop formation and emerging applications. *AIChE J.* 48(9):1842–48
Basaran OA, Gao H, Bhat PP. 2013. Nonstandard inkjets. *Annu. Rev. Fluid Mech.* 45:85–113
Bennacer R, Sefiane K. 2014. Vortices, dissipation and flow transition in volatile binary drops. *J. Fluid Mech.* 749:649–65
Beulen B, de Jong J, Reinten H, van den Berg M, Wijshoff H, van Dongen R. 2007. Flows on the nozzle plate of an inkjet printhead. *Exp. Fluids* 42:217–24
Bhat PP, Appathurai S, Harris MT, Pasquali M, McKinley GH, Basaran OA. 2010. Formation of beads-on-a-string structures during break-up of viscoelastic filaments. *Nat. Phys.* 6(8):625–31
Bonn D, Eggers J, Indekeu J, Meunier J, Rolley E. 2009. Wetting and spreading. *Rev. Mod. Phys.* 81(2):739–805
Boulogne F, Ingremeau F, Dervaux J, Limat L, Stone HA. 2015. Homogeneous deposition of particles by absorption on hydrogels. *EPL* 112(4):48004
Bouwhuis W, van der Veen RCA, Tran T, Keij DL, Winkels KG, et al. 2012. Maximal air bubble entrainment at liquid-drop impact. *Phys. Rev. Lett.* 109(26):264501
Brennen CE. 1995. *Cavitation and Bubble Dynamics*. Oxford: Oxford Univ. Press
Brenner MP, Hilgenfeldt S, Lohse D. 2002. Single bubble sonoluminescence. *Rev. Mod. Phys.* 74:425–84
Brenner MP, Lister JR, Stone HA. 1996. Pinching threads, singularities and the number 0.0304. . . *Phys. Fluids* 8(11):2827–36
Brenner MP, Shi XD, Nagel SR. 1994. Iterated instabilities during droplet fission. *Phys. Rev. Lett.* 73(25):3391–94
Brünahl J, Grishin AM. 2002. Piezoelectric shear mode drop-on-demand inkjet actuator. *Sens. Actuators A* 101(3):371–82
Bruning MA, Costalonga M, Karpitschka S, Snoeijer JH. 2018. Delayed coalescence of surfactant containing sessile droplets. *Phys. Rev. Fluids* 3(7):073605
Brutin D, Starov V. 2018. Recent advances in droplet wetting and evaporation. *Chem. Soc. Rev.* 47(2):558–85
Cai Y, Zhang-Newby BM. 2008. Marangoni flow-induced self-assembly of hexagonal and stripelike nanoparticle patterns. *J. Am. Chem. Soc.* 130(19):6076–77
Castrejon-Pita JR, Baxter W, Morgan J, Temple S, Martin G, Hutchings I. 2013. Future, opportunities and challenges of inkjet technologies. *At. Sprays* 23(6):541–65
Castrejón-Pita JR, Castrejón-Pita AA, Hinch EJ, Lister JR, Hutchings IM. 2012. Self-similar breakup of near-inviscid liquids. *Phys. Rev. E* 86(1):015301
Castrejón-Pita JR, Castrejón-Pita AA, Thete SS, Sambath K, Hutchings IM, et al. 2015. Plethora of transitions during breakup of liquid filaments. *PNAS* 112(15):4582–87
Castrejón-Pita JR, Morrison N, Harlen O, Martin G, Hutchings I. 2011. Experiments and Lagrangian simulations on the formation of droplets in drop-on-demand mode. *Phys. Rev. E* 83(3):036306
Cazabat AM, Guéna G. 2010. Evaporation of macroscopic sessile droplets. *Soft Matter* 6:2591–612
Christy JR, Hamamoto Y, Sefiane K. 2011. Flow transition within an evaporating binary mixture sessile drop. *Phys. Rev. Lett.* 106(20):205701
Cira NJ, Benusiglio A, Prakash M. 2015. Vapour-mediated sensing and motility in two-component droplets. *Nature* 519(7544):446–50
Clasen C, Phillips PM, Palangetic L, Vermant J. 2012. Dispensing of rheologically complex fluids: the map of misery. *AIChE J.* 58(10):3242–55
Craster RV, Matar OK. 2009. Dynamics and stability of thin liquid films. *Rev. Mod. Phys.* 81(3):1131–98
Daly RF, Harrington TS, Martin GD, Hutchings IM. 2015. Inkjet printing for pharmaceutics–a review of research and manufacturing. *Int. J. Pharm.* 494(2):554–67
Day RF, Hinch EJ, Lister JR. 1998. Self-similar capillary pinchoff of an inviscid fluid. *Phys. Rev. Lett.* 80:704–7
de Gans B, Duineveld PC, Schubert U. 2004. Ink jet printing of polymers: state of the art and future developments. *Adv. Mater.* 16:203–13

de Gennes PG. 1985. Wetting: statics and dynamics. *Rev. Mod. Phys.* 57:827–63

de Goede TC, de Bruin KG, Shahidzadeh N, Bonn D. 2019. Predicting the maximum spreading of a liquid drop impacting on a solid surface: effect of surface tension and entrapped air layer. *Phys. Rev. Fluids* 4(5):053602

de Jong J, Jeurissen R, Borel H, van den Berg M, Wijshoff H, et al. 2006a. Entrapped air bubbles in piezo-driven inkjet printing: their effect on the droplet velocity. *Phys. Fluids* 18:121511

de Jong J, Reinten H, van den Berg M, Wijshoff H, Versluis M, et al. 2006b. Air entrapment in piezo-driven inkjet nozzles. *J. Acoust. Soc. Am.* 120:1257–65

de Jong J, Reinten H, Wijshoff H, van den Berg M, Delescen K, et al. 2007. Marangoni flow on an inkjet nozzle plate. *Appl. Phys. Lett.* 91:204102

de Ruiter R, Colinet P, Brunet P, Snoeijer JH, Gelderblom H. 2017. Contact line arrest in solidifying spreading drops. *Phys. Rev. Fluids* 2(4):043602

Deegan RD, Bakajin O, Dupont TF, Huber G, Nagel SR, Witten TA. 1997. Capillary flow as the cause of ring stains from dried liquid drops. *Nature* 389(6653):827–29

Derby B. 2010. Inkjet printing of functional and structural materials: fluid property requirements, feature stability, and resolution. *Annu. Rev. Mater. Res.* 40:395–414

Diddens C. 2017. Detailed finite element method modeling of evaporating multi-component droplets. *J. Comput. Phys.* 340:670–87

Diddens C, Kuerten J, van der Geld C, Wijshoff H. 2017a. Modeling the evaporation of sessile multi-component droplets. *J. Colloid Inferface Sci.* 487:426–36

Diddens C, Tan H, Lv P, Versluis M, Kuerten JGM, et al. 2017b. Evaporating pure, binary and ternary droplets: thermal effects and axial symmetry breaking. *J. Fluid Mech.* 823:470–97

Dijksman JF. 1984. Hydrodynamics of small tubular pumps. *J. Fluid Mech.* 139:173–91

Dijksman JF. 1999. Hydro-acoustics of piezoelectrically driven ink-jet print heads. *Flow Turbul. Combust.* 61:211–37

Dijksman JF. 2019. *Design of Piezo Inkjet Print Heads: From Acoustics to Applications*. Weinheim, Ger.: Wiley-VCH

Dijksman JF, Duineveld PC, Hack MJJ, Pierik A, Rensen JM, et al. 2007. Precision ink jet printing of polymer light emitting displays. *J. Mater. Chem.* 17:511–22

Dong H, Carr WW, Morris JF. 2006. An experimental study of drop-on-demand drop formation. *Phys. Fluids* 18(7):072102

Dou R, Derby B. 2012. Formation of coffee stains on porous surfaces. *Langmuir* 28(12):5331–38

Driessen T, Jeurissen R. 2016. Drop formation in inkjet printing. In *Fundamentals of Inkjet Printing: The Science of Inkjet and Droplets*, ed. SD Hoath, pp. 93–115. Weinheim, Ger.: Wiley-VCH

Driessen T, Jeurissen R, Wijshoff H, Toschi F, Lohse D. 2013. Stability of viscous long liquid filaments. *Phys. Fluids* 25:062109

Driessen T, Sleutel P, Dijksman F, Jeurissen R, Lohse D. 2014. Control of jet breakup by a superposition of two Rayleigh-Plateau unstable modes. *J. Fluid Mech.* 749:275–96

Driscoll MM, Nagel SR. 2011. Ultrafast interference imaging of air in splashing dynamics. *Phys. Rev. Lett.* 107(15):154502

Driscoll MM, Stevens CS, Nagel SR. 2010. Thin film formation during splashing of viscous liquids. *Phys. Rev. E* 82(3):036302

Duchemin L, Eggers J, Josserand C. 2003. Inviscid coalescence of drops. *J. Fluid Mech.* 487:167–78

Duineveld PC. 2003. The stability of ink-jet printed lines of liquid with zero receding contact angle on a homogeneous substrate. *J. Fluid Mech.* 477:175–200

Eddi A, Winkels KG, Snoeijer JH. 2013. Influence of droplet geometry on the coalescence of low viscosity drops. *Phys. Rev. Lett.* 111:144502

Edwards A, Atkinson P, Cheung C, Liang H, Fairhurst D, Ouali F. 2018. Density-driven flows in evaporating binary liquid droplets. *Phys. Rev. Lett.* 121(18):184501

Eggers J. 1993. Universal pinching of 3D axisymmetric free-surface flow. *Phys. Rev. Lett.* 71(21):3458–60

Eggers J. 1997. Nonlinear dynamics and breakup of free-surface flows. *Rev. Mod. Phys.* 69(3):865–928

Eggers J. 2005. Drop formation—an overview. *Z. Angew. Math. Mech.* 85(6):400–10

Eggers J, Fontelos MA, Josserand C, Zaleski S. 2010. Drop dynamics after impact on a solid wall: theory and simulations. *Phys. Fluids* 22(6):062101
Eggers J, Lister JR, Stone HA. 1999. Coalescence of liquid drops. *J. Fluid Mech.* 401:293–310
Eggers J, Villermaux E. 2008. Physics of liquid jets. *Rep. Prog. Phys.* 71:036601
Erbil HY. 2012. Evaporation of pure liquid sessile and spherical suspended drops: a review. *Adv. Colloid Interface Sci.* 170(1–2):67–86
Feng JQ. 2002. A general fluid dynamic analysis of drop ejection in drop-on-demand ink jet devices. *J. Imaging Sci. Technol.* 46:398–408
Fraters A, Jeurissen R, van den Berg M, Reinten H, Wijshoff H, et al. 2020. Secondary tail formation and breakup in piezo-acoustic inkjet printing: femtoliter droplets captured in flight. *Phys. Rev. Appl.* 13:024075
Fraters A, Segers T, van den Berg M, Reinten H, Wijshoff H, et al. 2019a. Shortwave infrared imaging setup to study entrained air bubble dynamics in a MEMS-based piezo-acoustic inkjet printhead. *Exp. Fluids* 60(8):123
Fraters A, van den Berg M, de Loore Y, Reinten H, Wijshoff H, et al. 2019b. Inkjet nozzle failure by heterogeneous nucleation: bubble entrainment, cavitation, and diffusive growth. *Phys. Rev. Appl.* 12(6):064019
Funakubo H, Dekkers M, Sambri A, Gariglio S, Shklyarevskiy I, Rijnders G. 2012. Epitaxial PZT films for MEMS printing applications. *MRS Bull.* 37(11):1030–38
Gambaryan-Roisman T. 2014. Liquids on porous layers: wetting, imbibition and transport processes. *Curr. Opin. Colloid Interface Sci.* 19(4):320–35
Garcia-Sucerquia J, Xu W, Jericho S, Klages P, Jericho M, Kreuzer H. 2006. Digital in-line holographic microscopy. *Appl. Opt.* 45(5):836–50
Gaver DP, Grotberg JB. 1992. Droplet spreading on a thin viscous film. *J. Fluid Mech.* 235:399–414
Giorgiutti-Dauphiné F, Pauchard L. 2018. Drying drops. *Eur. Phys. J. E* 41(3):32
Gomez H, Hughes T, Nogueira X, Calo V. 2010. Isogeometric analysis of the isothermal Navier–Stokes–Korteweg equations. *Comput. Methods Appl. Mech. Eng.* 199:1828–40
Gordillo JM, Riboux G, Quintero ES. 2019. A theory on the spreading of impacting droplets. *J. Fluid Mech.* 866:298–315
Hack M, Costalonga M, Segers T, Karpitschka S, Wijshoff H, Snoeijer J. 2018. Printing wet-on-wet: attraction and repulsion of drops on a viscous film. *Appl. Phys. Lett.* 113(18):183701
Han W, Lin Z. 2012. Learning from coffee rings: ordered structures enabled by controlled evaporative self-assembly. *Angew. Chem. Int. Ed.* 51(7):1534–46
Harting J, Frijters S, Ramaioli M, Robinson M, Wolf DE, Luding S. 2014. Recent advances in the simulation of particle-laden flows. *Eur. Phys. J. Spec. Top.* 223:2253–67
Heil M, Hazel AL. 2006. oomph-lib—an *o*bject-*o*riented *m*ulti-*ph*ysics finite-element *lib*rary. In *Fluid-Structure Interaction*, ed. H-J Bungartz, M Schäfer, pp. 19–49. Berlin: Springer
Heil M, Hazel AL. 2011. Fluid-structure interaction in internal physiological flows. *Annu. Rev. Fluid Mech.* 43:141–62
Hell SW. 2009. Microscopy and its focal switch. *Nat. Methods* 6(1):24–32
Hernandez-Sanchez JF, Lubbers LA, Eddi A, Snoeijer JH. 2012. Symmetric and asymmetric coalescence of drops on a substrate. *Phys. Rev. Lett.* 109:184502
Hessling D, Xie Q, Harting J. 2017. Diffusion dominated evaporation in multicomponent Lattice-Boltzmann simulations. *J. Chem. Phys.* 146(5):054111
Hicks PD, Purvis R. 2010. Air cushioning and bubble entrapment in three-dimensional droplet impacts. *J. Fluid Mech.* 649:135–63
Hicks PD, Purvis R. 2011. Air cushioning in droplet impacts with liquid layers and other droplets. *Phys. Fluids* 23(6):062104
Hoath SD, ed. 2016. *Fundamentals of Inkjet Printing: The Science of Inkjet and Droplets*. Weinheim, Ger.: Wiley-VCH
Hoath SD, Harlen OG, Hutchings IM. 2012. Jetting behavior of polymer solutions in drop-on-demand inkjet printing. *J. Rheol.* 56(5):1109–27
Hu H, Larson RG. 2005. Analysis of the effects of Marangoni stresses on the microflow in an evaporating sessile droplet. *Langmuir* 21(9):3972–80

Hutchings I, Martin G, Hoath S. 2007. High speed imaging and analysis of jet and drop formation. *J. Imaging Sci. Technol.* 51(5):438–44
Jacqmin D. 1999. Calculation of two-phase Navier-Stokes flows using phase-field modeling. *J. Comput. Phys.* 155(1):96–127
Jacqmin D. 2000. Contact-line dynamics of a diffuse fluid interface. *J. Fluid Mech.* 402:57–88
Jalaal M, Seyfert C, Stoeber B, Balmforth N. 2018. Gel-controlled droplet spreading. *J. Fluid Mech.* 837:115–28
Jehannin M, Charton S, Karpitschka S, Zemb T, Moehwald H, Riegler H. 2015. Periodic precipitation patterns during coalescence of reacting sessile droplets. *Langmuir* 31(42):11484–90
Jeurissen R, de Jong J, Reinten H, van den Berg M, Wijshoff H, et al. 2008. Effect of an entrained air bubble on the acoustics of an ink channel. *J. Acoust. Soc. Am.* 123(5):2496–505
Jeurissen R, van der Bos A, Reinten H, van den Berg M, Wijshoff H, et al. 2009. Acoustic measurement of bubble size in an inkjet printhead. *J. Acoust. Soc. Am.* 126(5):2184–90
Josserand C, Popinet S, Zaleski S. 2009. Numerical simulation of droplets, bubbles and waves: state of the art. *Fluid Dyn. Res.* 41:065001
Josserand C, Thoroddsen S. 2016. Drop impact on a solid surface. *Annu. Rev. Fluid Mech.* 48:365–91
Kamat PM, Wagoner BW, Castrejón-Pita AA, Castrejón-Pita JR, Anthony CR, Basaran OA. 2020. Surfactant-driven escape from endpinching during contraction of nearly inviscid filaments. *J. Fluid Mech* 899:A28
Kamat PM, Wagoner BW, Thete SS, Basaran OA. 2018. Role of Marangoni stress during breakup of surfactant-covered liquid threads: reduced rates of thinning and microthread cascades. *Phys. Rev. Fluids* 3(4):043602
Kant P, Hazel AL, Dowling M, Thompson AB, Juel A. 2017. Controlling droplet spreading with topography. *Phys. Rev. Fluids* 2(9):094002
Kant P, Koldeweij RB, Harth K, van Limbeek MA, Lohse D. 2020. Fast-freezing kinetics inside a droplet impacting on a cold surface. *PNAS* 117(6):2788–94
Kaplan CN, Mahadevan L. 2015. Evaporation-driven ring and film deposition from colloidal droplets. *J. Fluid Mech.* 781:R2
Kapur N, Gaskell PH. 2007. Morphology and dynamics of droplet coalescence on a surface. *Phys. Rev. E* 75:056315
Karpitschka S. 2018. The value of a fading tracer. *J. Fluid Mech.* 856:1–4
Karpitschka S, Liebig F, Riegler H. 2017. Marangoni contraction of evaporating sessile droplets of binary mixtures. *Langmuir* 33(19):4682–87
Karpitschka S, Riegler H. 2010. Quantitative experimental study on the transition between fast and delayed coalescence of sessile droplets with different but completely miscible liquids. *Langmuir* 26(14):11823–29
Karpitschka S, Riegler H. 2012. Noncoalescence of sessile drops from different but miscible liquids: hydrodynamic analysis of the twin drop contour as a self-stabilizing traveling wave. *Phys. Rev. Lett.* 109(6):066103
Karpitschka S, Riegler H. 2014. Sharp transition between coalescence and non-coalescence of sessile drops. *J. Fluid Mech.* 743:R1
Kateri EP, William SW, Steven ER, Robert AS. 2003. Additive jet printing of polymer thin-film transistors. *Appl. Phys. Lett.* 83:2070–72
Keshavarz B, Sharma V, Houze EC, Koerner MR, Moore JR, et al. 2015. Studying the effects of elongational properties on atomization of weakly viscoelastic solutions using Rayleigh Ohnesorge Jetting Extensional Rheometry (ROJER). *J. Non-Newton. Fluid Mech.* 222:171–89
Kim H, Boulogne F, Um E, Jacobi I, Button E, Stone HA. 2016. Controlled uniform coating from the interplay of Marangoni flows and surface-adsorbed macromolecules. *Phys. Rev. Lett.* 116(12):124501
Kim H, Muller K, Shardt O, Afkhami S, Stone HA. 2017. Solutal Marangoni flows of miscible liquids drive transport without surface contamination. *Nat. Phys.* 13(11):1105–10
Kim H, Stone HA. 2018. Direct measurement of selective evaporation of binary mixture droplets by dissolving materials. *J. Fluid Mech.* 850:769–83
Kim J, Kang K, Lowengrub J. 2004. Conservative multigrid methods for Cahn–Hilliard fluids. *J. Comput. Phys.* 193:511–43
Kim P, Wong TS, Alvarenga J, Kreder MJ, Adorno-Martinez WE, Aizenberg J. 2012. Liquid-infused nanostructured surfaces with extreme anti-ice and anti-frost performance. *ACS Nano* 6(8):6569–77

Kolinski JM, Rubinstein SM, Mandre S, Brenner MP, Weitz DA, Mahadevan L. 2012. Skating on a film of air: drops impacting on a surface. *Phys. Rev. Lett.* 108(7):074503
Kuang M, Wang L, Song Y. 2014. Controllable printing droplets for high-resolution patterns. *Adv. Mater.* 26(40):6950–58
Laan N, de Bruin KG, Bartolo D, Josserand C, Bonn D. 2014. Maximum diameter of impacting liquid droplets. *Phys. Rev. Appl.* 2(4):044018
Lamb H. 1932. *Hydrodynamics*. Cambridge, UK: Cambridge Univ. Press
Le HP. 1998. Progress and trends in ink-jet printing technology. *J. Imaging Sci. Technol.* 42:49–62
Lee J, Laan N, de Bruin KG, Skantzaris G, Shahidzadeh N, et al. 2016. Universal rescaling of drop impact on smooth and rough surfaces. *J. Fluid Mech.* 786:R4
Lee M, Kang DK, Yoon SS, Yarin AL. 2012. Coalescence of two drops on partially wettable substrates. *Langmuir* 28:3791–98
Li Y, Diddens C, Lv P, Wijshoff H, Versluis M, Lohse D. 2019a. Gravitational effect in evaporating binary microdroplets. *Phys. Rev. Lett.* 122(11):114501
Li Y, Diddens C, Prosperetti A, Chong KL, Zhang X, Lohse D. 2019b. Bouncing oil droplet in a stratified liquid and its sudden death. *Phys. Rev. Lett.* 122(15):154502
Li Y, Diddens C, Segers T, Wijshoff H, Versluis M, Lohse D. 2020a. Evaporating droplets on oil-wetted surfaces: suppression of the coffee-stain effect. *PNAS* 117(29):16756–63
Li Y, Lv P, Diddens C, Tan H, Wijshoff H, et al. 2018. Evaporation-triggered segregation of sessile binary droplets. *Phys. Rev. Lett.* 120:224501
Li Y, Salvator V, Wijshoff H, Versluis M, Lohse D. 2020b. Evaporation-induced crystallization of surfactants in sessile multicomponent droplets. *Langmuir* 36(26):7545–52
Lin S, Zhao B, Zou S, Guo J, Wei Z, Chen L. 2018. Impact of viscous droplets on different wettable surfaces: impact phenomena, the maximum spreading factor, spreading time and post-impact oscillation. *J. Colloid Interface Sci.* 516:86–97
Lin SP, Reitz RD. 1998. Drop and spray formation from a liquid jet. *Annu. Rev. Fluid Mech.* 30:85–105
Liu J, Gomez H, Evans J, Hughes T, Landis C. 2013. Functional entropy variables: a new methodology for deriving thermodynamically consistent algorithms for complex fluids, with particular reference to the isothermal Navier–Stokes–Korteweg equations. *J. Comput. Phys.* 248:47–86
Liu Y, Derby B. 2019. Experimental study of the parameters for stable drop-on-demand inkjet performance. *Phys. Fluids* 31(3):032004
Lohse D. 2018. Bubble puzzles: from fundamentals to applications. *Phys. Rev. Fluids* 3(10):110504
Lohse D, Zhang X. 2015. Surface nanobubble and surface nanodroplets. *Rev. Mod. Phys.* 87:981–1035
Lohse D, Zhang X. 2020. Physicochemical hydrodynamics of droplets out of equilibrium. *Nat. Rev. Phys.* 2:426–43
Louvet N, Bonn D, Kellay H. 2014. Nonuniversality in the pinch-off of yield stress fluids: role of nonlocal rheology. *Phys. Rev. Lett.* 113(21):218302
Magen E, Gottlieb M. 2004. The importance of liquid compressibility in calculations of fluid dynamics inside a DOD piezoelectric ink jet nozzle. *J. Imaging Sci. Technol.* 48:335–41
Mandre S, Brenner MP. 2012. The mechanism of a splash on a dry solid surface. *J. Fluid Mech.* 690:148–72
Mandre S, Mani M, Brenner MP. 2009. Precursors to splashing of liquid droplets on a solid surface. *Phys. Rev. Lett.* 102(13):134502
Mani M, Mandre S, Brenner MP. 2010. Events before droplet splashing on a solid surface. *J. Fluid Mech.* 647:163–85
Manikantan H, Squires TM. 2020. Surfactant dynamics: hidden variables controlling fluid flows. *J. Fluid Mech.* 892:P1
Marin A, Karpitschka S, Noguera-Marn D, Cabrerizo-Vlchez MA, Rossi M, et al. 2019. Solutal Marangoni flow as the cause of ring stains from drying salty colloidal drops. *Phys. Rev. Fluids* 4(4):041601
Marin AG, Gelderblom H, Lohse D, Snoeijer JH. 2011. Order-to-disorder transition in ring-shaped colloidal stains. *Phys. Rev. Lett.* 107:085502
Marin AG, Liepelt R, Rossi M, Kähler CJ. 2016. Surfactant-driven flow transitions in evaporating droplets. *Soft Matter* 12(5):1593–600

Martin GD, Hoath SD, Hutchings IM. 2008. Inkjet printing-the physics of manipulating liquid jets and drops. *J. Phys. Conf. Ser* 105:012001
McIlroy C, Harlen OG. 2019. Effects of drive amplitude on continuous jet break-up. *Phys. Fluids* 31(6):064104
McKinley GH, Renardy M. 2011. Wolfgang von Ohnesorge. *Phys. Fluids* 23(12):127101
Meacham JM, Varady MJ, Degertekin FL, Fedorov AG. 2005. Droplet formation and ejection from a micromachined ultrasonic droplet generator: Visualization and scaling. *Phys. Fluids* 17:100605
Motaghian M, Shirsavar R, Erfanifam M, Sabouhi M, van der Linden E, et al. 2019. Rapid spreading of a droplet on a thin soap film. *Langmuir* 35(46):14855–60
Mundo C, Sommerfeld M, Tropea C. 1995. Droplet-wall collisions: experimental studies of the deformation and breakup process. *Int. J. Multiph. Flow* 21(2):151–73
Notz PK, Basaran OA. 2004. Dynamics and breakup of a contracting liquid filament. *J. Fluid Mech.* 512:223–56
Oron A, Davis SH, Bankoff SG. 1997. Long-scale evolution of thin liquid films. *Rev. Mod. Phys.* 69(3):931–81
Pack M, Hu H, Kim DO, Yang X, Sun Y. 2015. Colloidal drop deposition on porous substrates: competition among particle motion, evaporation, and infiltration. *Langmuir* 31(29):7953–61
Pack M, Hu H, Kim DO, Zheng Z, Stone H, Sun Y. 2017. Failure mechanisms of air entrainment in drop impact on lubricated surfaces. *Soft Matter* 13(12):2402–9
Papageorgiou DT. 1995. On the breakup of viscous liquid threads. *Phys. Fluids* 7(7):1529–44
Paulsen JD, Burton JC, Nagel SR. 2011. Viscous to inertial crossover in liquid drop coalescence. *Phys. Rev. Lett.* 106:114501
Pham T, Kumar S. 2019. Imbibition and evaporation of droplets of colloidal suspensions on permeable substrates. *Phys. Rev. Fluids* 4(3):034004
Picknett RG, Bexon R. 1977. The evaporation of sessile or pendant drops in still air. *J. Colloid Interface Sci.* 61:336–50
Popinet S. 2018. Numerical models of surface tension. *Annu. Rev. Fluid Mech.* 50:49–75
Qian J, Law CK. 1997. Regimes of coalescence and separation in droplet collision. *J. Fluid Mech.* 331:59–80
Quéré D. 2008. Wetting and roughness. *Annu. Rev. Mater. Sci.* 38:71–99
Quéré D. 2013. Leidenfrost dynamics. *Annu. Rev. Fluid Mech.* 45:197–215
Riboux G, Gordillo JM. 2014. Experiments of drops impacting a smooth solid surface: a model of the critical impact speed for drop splashing. *Phys. Rev. Lett.* 113(2):024507
Ristenpart WD, Kim PG, Domingues C, Wan J, Stone HA. 2007. Influence of substrate conductivity on circulation reversal in evaporating drops. *Phys. Rev. Lett.* 99(23):234502
Ristenpart WD, McCalla PM, Roy RV, Stone HA. 2006. Coalescence of spreading droplets on a wettable substrate. *Phys. Rev. Lett.* 97:064501
Sambath K, Garg V, Thete SS, Subramani HJ, Basaran OA. 2019. Inertial impedance of coalescence during collision of liquid drops. *J. Fluid Mech.* 876:449–80
Schäfle C, Bechinger C, Rinn B, David C, Leiderer P. 1999. Cooperative evaporation in ordered arrays of volatile droplets. *Phys. Rev. Lett.* 82:5302–5
Schofield F, Wilson S, Pritchard D, Sefiane K. 2018. The lifetimes of evaporating sessile droplets are significantly extended by strong thermal effects. *J. Fluid Mech.* 851:231–44
Schulkes R. 1996. The contraction of liquid filaments. *J. Fluid Mech.* 309:277–300
Scriven L, Sternling C. 1960. The Marangoni effects. *Nature* 187(4733):186–88
Sefiane K. 2014. Patterns from drying drops. *Adv. Colloid Interface Sci.* 206:372–81
Seppecher P. 1996. Moving contact lines in the Cahn-Hilliard theory. *Int. J. Eng. Sci.* 34:977–92
Shi XD, Brenner MP, Nagel SR. 1994. A cascade of structure in a drop falling from a faucet. *Science* 265(5169):219–22
Shin DY, Grassia P, Derby B. 2003. Oscillatory limited compressible fluid flow induced by the radial motion of a thick-walled piezoelectric tube. *J. Acoust. Soc. Am.* 114:1314–21
Shirota M, van Limbeek MA, Sun C, Prosperetti A, Lohse D. 2016. Dynamic Leidenfrost effect: relevant time and length scales. *Phys. Rev. Lett.* 116(6):064501
Sirringhaus H, Kawase T, Friend R, Shimoda T, Inbasekaran M, et al. 2000. High-resolution inkjet printing of all-polymer transistor circuits. *Science* 290(5499):2123–26
Snoeijer JH, Andreotti B. 2013. Moving contact lines: scales, regimes, and dynamical transitions. *Annu. Rev. Fluid Mech.* 45:269–92

Staat HJ, van der Bos A, van den Berg M, Reinten H, Wijshoff H, et al. 2017. Ultrafast imaging method to measure surface tension and viscosity of inkjet-printed droplets in flight. *Exp. Fluids* 58:2

Stauber JM, Wilson SK, Duffy BR, Sefiane K. 2014. On the lifetimes of evaporating droplets. *J. Fluid Mech.* 744:R2

Stone HA. 1994. Dynamics of drop deformation and breakup in viscous fluids. *Annu. Rev. Fluid Mech.* 26:65–102

Sui Y, Maglio M, Spelt PDM, Legendre D, Ding H. 2013. Inertial coalescence of droplets on a partially wetting substrate. *Phys. Fluids* 25(10):101701

Sykes TC, Castrejón-Pita AA, Castrejón-Pita JR, Harbottle D, Khatir Z, et al. 2020. Surface jets and internal mixing during the coalescence of impacting and sessile droplets. *Phys. Rev. Fluids* 5(2):023602

Talbot E, Berson A, Brown P, Bain C. 2012. Evaporation of picoliter droplets on surfaces with a range of wettabilities and thermal conductivities. *Phys. Rev. E* 85(6):061604

Tan H, Diddens C, Lv P, Kuerten JGM, Zhang X, Lohse D. 2016. Evaporation-triggered microdroplet nucleation and the four life phases of an evaporating ouzo drop. *PNAS* 113:8642–47

Tang X, Saha A, Law CK, Sun C. 2019. Bouncing drop on liquid film: dynamics of interfacial gas layer. *Phys. Fluids* 31:013304

Tanner L. 1979. The spreading of silicone oil drops on horizontal surfaces. *J. Phys. D* 12:1473–84

Thoroddsen ST, Etoh TG, Takehara K. 2003. Air entrapment under an impacting drop. *J. Fluid Mech.* 478:125–34

Thoroddsen ST, Etoh TG, Takehara K. 2008. High-speed imaging of drops and bubbles. *Annu. Rev. Fluid Mech.* 40:257–85

Thoroddsen ST, Etoh TG, Takehara K, Ootsuka N, Hatsuki A. 2005. The air bubble entrapped under a drop impacting on a solid surface. *J. Fluid Mech.* 545:203–12

Tijdeman H. 1975. On the propagation of sound waves in cylindrical tubes. *J. Sound Vibr.* 39:1–33

Tirtaatmadja V, McKinley GH, Cooper-White JJ. 2006. Drop formation and breakup of low viscosity elastic fluids: effects of molecular weight and concentration. *Phys. Fluids* 18(4):043101

Tran T, Staat HJJ, Prosperetti A, Sun C, Lohse D. 2012. Drop impact on superheated surfaces. *Phys. Rev. Lett.* 108(3):036101

Tsai P, Hendrix MHW, Dijkstra RM, Shui L, Lohse D. 2011. Microscopic structure influencing macroscopic splash at high Weber number. *Soft Matter* 7(24):11325–33

Tsai P, van der Veen RCA, van de Raa M, Lohse D. 2010. How micropatterns and air pressure affect splashing on surfaces. *Langmuir* 26:16090–95

van Brummelen E, Shokrpour-Roudbari M, Van Zwieten G. 2016. Elasto-capillarity simulations based on the Navier–Stokes–Cahn–Hilliard equations. In *Advances in Computational Fluid-Structure Interaction and Flow Simulation*, ed. Y Bazilevs, K Takizawa, pp. 451–62. Berlin: Springer

van Dam DB, Clerc CL. 2004. Experimental study of the impact of an ink-jet printed droplet on a solid substrate. *Phys. Fluids* 16(9):3403–14

van der Bos A, Segers T, Jeurissen R, van den Berg M, Reinten H, et al. 2011a. Infrared imaging and acoustic sizing of a bubble inside a micro-electro-mechanical system piezo ink channel. *J. Appl. Phys.* 110:034503

van der Bos A, van der Meulen MJ, Driessen T, van den Berg M, Reinten H, et al. 2014. Velocity profile inside piezoacoustic inkjet droplets in flight: comparison between experiment and numerical simulation. *Phys. Rev. Appl.* 1:014004

van der Bos A, Zijlstra A, Gelderblom E, Versluis M. 2011b. iLIF: illumination by laser-induced fluorescence for single flash imaging on a nanoseconds timescale. *Exp. Fluids* 51(5):1283–89

van der Meulen MJ, Reinten H, Wijshoff H, Versluis M, Lohse D, Steen P. 2020. Nonaxisymmetric effects in drop-on-demand piezoacoustic inkjet printing. *Phys. Rev. Appl.* 13(5):054071

van der Veen RCA, Tran T, Lohse D, Sun C. 2012. Direct measurements of air layer profiles under impacting droplets using high-speed color interferometry. *Phys. Rev. E* 85:026315

van Gaalen R, Diddens C, Wijshoff H, Kuerten J. 2021. Marangoni circulation in evaporating droplets in the presence of soluble surfactants. *J. Colloid Interface Sci.* 584:622–33

van Hoeve W, Gekle S, Snoeijer J, Versluis M, Brenner MP, Lohse D. 2010. Breakup of diminutive Rayleigh jets. *Phys. Fluids* 22:122003

Vazquez G, Alvarez E, Navaza JM. 1995. Surface tension of alcohol water + water from 20 to 50 °C. *J. Chem. Eng. Data* 40(3):611–14
Versluis M. 2013. High-speed imaging in fluids. *Exp. Fluids* 54:1458
Visser CW, Frommhold PE, Wildeman S, Mettin R, Lohse D, Sun C. 2015. Dynamics of high-speed micro-drop impact: numerical simulations and experiments at frame-to-frame times below 100 ns. *Soft Matter* 11(9):1708–22
Visser CW, Kamperman T, Karbaat LP, Lohse D, Karperien M. 2018. In-air microfluidics enables rapid fabrication of emulsions, suspensions, and 3D modular (bio)materials. *Sci. Adv.* 4(1):eaao1175
Wang S, Zhong Y, Fang H. 2019. Deformation characteristics of a single droplet driven by a piezoelectric nozzle of the drop-on-demand inkjet system. *J. Fluid Mech.* 869:634–45
Wang Z, Karapetsas G, Valluri P, Sefiane K, Williams A, et al. 2021. Dynamics of hygroscopic aqueous solution droplets undergoing evaporation vapour absorption. *J. Fluid Mech.* 912:A2
Wee H, Wagoner BW, Kamat PM, Basaran OA. 2020. Effects of surface viscosity on breakup of viscous threads. *Phys. Rev. Lett.* 124(20):204501
Wijshoff H. 2010. The dynamics of the piezo inkjet printhead operation. *Phys. Rep.* 491(4–5):77–177
Wijshoff H. 2018. Drop dynamics in the inkjet printing process. *Cur. Opin. Colloid Interface Sci.* 36:20–27
Wildeman S, Visser CW, Sun C, Lohse D. 2016. On the spreading of impacting drops. *J. Fluid Mech.* 805:636–55
Williams AGL, Karapetsas G, Mamalis D, Sefiane K, Matar OK, Valluri P. 2021. Spreading and retraction dynamics of sessile evaporating droplets comprising volatile binary mixtures. *J. Fluid Mech.* 907:A22
Williams C. 2006. Ink-jet printers go beyond paper. *Phys. World* 19(1):24–29
Wray AW, Duffy BR, Wilson SK. 2020. Competitive evaporation of multiple sessile droplets. *J. Fluid Mech.* 884:A45
Xu L. 2007. Liquid drop splashing on smooth, rough, and textured surfaces. *Phys. Rev. E* 75(5):056316
Xu L, Barcos L, Nagel SR. 2007. Splashing of liquids: interplay of surface roughness with surrounding gas. *Phys. Rev. E* 76(6):066311
Xu L, Shi T, An L. 2007. Nonsolvent-induced dewetting of thin polymer films. *Langmuir* 23(18):9282–86
Xu L, Zhang WW, Nagel SR. 2005. Drop splashing on a dry smooth surface. *Phys. Rev. Lett.* 94(18):184505
Xu Q, Basaran OA. 2007. Computational analysis of drop-on-demand drop formation. *Phys. Fluids* 19(10):102111
Yarin AL. 2006. Drop impact dynamics: splashing, spreading, receding, bouncing.... *Annu. Rev. Fluid Mech.* 38:159–92
Yarin AL, Roisman IV, Tropea C. 2017. *Collision Phenomena in Liquids and Solids*. Cambridge, UK: Cambridge Univ. Press
Zang D, Tarafdar S, Tarasevich YY, Choudhury MD, Dutta T. 2019. Evaporation of a droplet: from physics to applications. *Phys. Rep.* 804:1–56
Zapka W, ed. 2017. *Handbook of Industrial Inkjet Printing: A Full System Approach*. Weinhein, Ger.: Wiley-VCH
Zhang LV, Brunet P, Eggers J, Deegan RD. 2010. Wavelength selection in the crown splash. *Phys. Fluids* 22(12):122105
Zhang X, Basaran OA. 1997. Dynamic surface tension effects in impact of a drop with a solid surface. *J. Colloid Interface Sci.* 187(1):166–78
Zhang XH, Wang J, Bao L, Dietrich E, van der Veen RCA, et al. 2015. Mixed mode of dissolving immersed nanodroplets at a solid-water interface. *Soft Matter* 11:1889–900
Zhong Y, Fang H, Ma Q, Dong X. 2018. Analysis of droplet stability after ejection from an inkjet nozzle. *J. Fluid Mech.* 845:378–91

Annual Review of Fluid Mechanics

Volume 54, 2022

Contents

Indexes

Errata

An online log of corrections to *Annual Review of Fluid Mechanics* articles may be found at http://www.annualreviews.org/errata/fluid